Acta Geologica Polonica, Vol. 64 (2014), No. 4, pp. 473–494
DOI: 10.2478/agp-2014-0025

Alteration of mélange-hosted chromitites from Korydallos, Pindos ophiolite complex, Greece: evidence for modification by a residual high-T post-magmatic fluid

ARGYRIOS N. KAPSIOTIS

Department of Geology, Section of Earth Materials, Panepistimiopolis of Rion, University of Patras, 265 04 Patras, Greece
School of Earth Science and Geological Engineering, Sun Yat-sen University, Guangzhou 510275, P. R. of China [Current address].
E-mail: kapsiotisa@yahoo.gr

ABSTRACT:

Kapsiotis, A.N. 2014. Alteration of mélange-hosted chromitites from Korydallos, Pindos ophiolite complex, Greece: evidence for modification by a residual high-T post-magmatic fluid. *Acta Geologica Polonica*, **64** (4), 473–494. Warszawa.

The peridotites from the area of Korydallos, in the Pindos ophiolitic massif, crop out as deformed slices of a rather dismembered sub-oceanic, lithospheric mantle section and are tectonically enclosed within the Avdella mélange. The most sizeable block is a chromitite-bearing serpentinite showing a mesh texture. Accessory, subhedral to euhedral Cr-spinels in the serpentinite display Cr# [Cr/(Cr + Al)] values that range from 0.36 to 0.42 and Mg# [Mg/(Mg + Fe^{2+})] values that vary between 0.57 and 0.62, whereas the TiO_2 content may be up to 0.47 wt.%. The serpentinite fragment is characterized by low abundances of magmaphile elements (Al_2O_3: 0.66 wt.%, CaO: 0.12 wt.%, Na_2O: 0.08 wt.%, TiO_2: 0.007 wt.%, Sc: 4 ppm) and enrichment in compatible elements (Cr: 2780 ppm and Ni: 2110 ppm). Overall data are in accordance with derivation of the serpentinite exotic block from a dunite that was formed in the mantle region underneath a back-arc basin before tectonic incorporation in the Korydallos mélange.

Two compositionally different chromitite pods are recognized in the studied serpentinite fragment, a Cr-rich chromitite and a high-Al chromitite, which have been ascribed to crystallization from a single, progressively differentiating MORB/IAT melt. Although both pods are fully serpentinized only the Al-rich one shows signs of limited Cr-spinel replacement by an opaque spinel phase and clinochlore across grain boundaries and fractures. Modification of the ore-making Cr-spinel is uneven among the Al-rich chromitite specimens. Textural features such as olivine replacement by clinochlore and clinochlore disruption by serpentine indicate that Cr-spinel alteration is not apparently related to serpentinization. From the unaltered Cr-spinel cores to their reworked boundaries the Al_2O_3 and MgO abundances decrease, being mainly compensated by FeO^t and Cr_2O_3 increases. Such compositional variations are suggestive of restricted ferrian chromite (and minor magnetite) substitution for Cr-spinel during a short-lived but relatively intense, low amphibolite facies metamorphic episode (temperature: 400–700 °C). The presence of tremolite and clinochlore in the interstitial groundmass of the high-Al chromitite and their absence from the Cr-rich chromitite matrix imply that after chromitite formation a small volume of a high temperature, post-magmatic fluid reacted with Cr-spinel, triggering its alteration.

Key words: Ferrian chromite; Cr-spinel; Metamorphism; Ophiolites; Pindos.

INTRODUCTION

Chromian spinel [Cr-spinel: $(Mg,Fe^{2+})(Cr,Al,Fe^{3+})_2O_4$] is a valuable mineral that may help in understanding the petrological processes involved in the formation and evolution of the Earth's upper mantle. It is commonly referred to as a petrogenetic indicator since its chemistry is believed to be strongly dependent on the degree of mantle melting and the compositional signature of the partial melt generated (e.g., Dick and Bullen 1984; Proenza *et al*. 1999; Hellebrand *et al*. 2001; Kamenetsky *et al*. 2001; Zhou *et al*. 2005; Ahmed *et al*. 2012; Azer 2014; Xiong *et al*. 2014). Due to its refractory nature it is highly resistant to long-standing post-magmatic processes, such as hydrothermal alteration, and to metamorphism. Nevertheless, it is currently accepted that even primary Cr-spinel may undergo significant textural and compositional modification in the low T alteration regime (e.g., Ulmer 1974; Kimball 1990; Barnes 2000; Mellini *et al*. 2005; González-Jiménez *et al*. 2009; Teixeira *et al*. 2012). In addition, it is currently recognized that even a hydrothermal origin is possible for Cr-spinel in ultramafic rocks that have experienced fluid activity, assuming that there was sufficient Cr-spinel at the fluid source (Arai and Akizawa 2014). Therefore, Cr-spinel compositional data should always be treated with caution, especially in intensely altered and deformed mantle peridotites and podiform chromitites (e.g., Arai *et al*. 2006).

Many recent studies support the suggestion that ferrian chromite $[(Fe^{2+},Fe^{3+},Mg)(Cr,Fe^{3+},Fe^{2+},Al)_2O_4]$ is the most common alteration product of Cr-spinel, characterized by a significant increase in the Cr/Al ratio and Fe^{3+} content and by a substantial decrease in the Mg/Fe^{2+} ratio (e.g., Wylie *et al*. 1987; Merlini *et al*. 2009; Mukherjee *et al*. 2010; Derbyshire *et al*. 2013). However, the exact origin, extent and relative timing of Cr-spinel alteration remain hotly debated issues. Frequently, serpentinization (e.g., Burkhard 1993), weathering (e.g., Economou-Eliopoulos 2003) and metamorphism (e.g., Singh and Singh 2013) are considered to be processes responsible for the growth of ferrian chromite at the expense of primary Cr-spinel. Such replacement is commonly concentric, beginning at grain boundaries and brittle cracks and advancing inwards (e.g., Saumur and Hattori 2013), although sometimes it may follow rather irregular patterns (e.g., Gervilla *et al*. 2012). The development of these zoning patterns in Cr-spinel in relation to alteration and/or metamorphism can provide important constraints on identifying the sequence of post-magmatic events affecting the mantle formations (e.g., Merlini *et al*. 2009; Colás *et al*. 2012).

In the present paper the effects of serpentinization and metamorphism on the texture and composition of Cr-spinels from a set of podiform chromitites hosted in an exotic serpentinite block from the Korydallos mélange, Pindos ophiolitic massif, are discussed. The current study also attempts to provide insights into the origin of the peridotite fragment, aiming to contribute to a more thorough understanding of the petrogenetic evolution of the Pindos oceanic mantle.

GENERAL GEOLOGICAL SETTING

The Albanian-Pindos cordillera was generated as a result of the convergence between the Apulia and Pelagonian (Cimmerian) microcontinents during the Late Cretaceous-Eocene. It represents a collisional orogenic belt formed by a series of west-trending thrust sheets and folds that verge towards the WSW (Robertson *et al*. 1991). In Greece the cordillera is made up by formations that belong to the Pindos and Subpelagonian isopic zones, whereas the boundary between them is marked by ophiolite occurrences that crop out as a NNW-SSE oriented belt (e.g., Beccaluva *et al*. 1984). Ophiolite exposures in central continental Greece occur in the form of a separate nappe, commonly referred to as the Jurassic-Early Cretaceous 'Eohellenic nappe' (Jacobshagen 1986; Text-fig. 1a). The Eohellenic ophiolites are interpreted as lithospheric remnants of the Neo-Tethyan Pindos oceanic basin that were tectonically emplaced onto the Pelagonian passive continental margin (e.g., Robertson *et al*. 1991; Robertson 2002; Bortolotti *et al*. 2004; Saccani *et al*. 2008). Among the Eohellenic ophiolites the Pindos ophiolite complex constitutes part of the homonymous isopic zone, which consists of a sequence of Tertiary nappes, lying towards the WSW over the flysch of the Ionian and Gavrovo zones (Brunn 1956). Jones and Robertson (1991) described the tectono-stratigraphic structure of the Pindos zone as made up of the following principal tectonic units: 1) the Middle to Upper Jurassic Pindos ophiolitic nappe, 2) the shallow-water Orliakas limestones (Late Cretaceous), 3) the Avdella sub-ophiolitic mélange (Late Triassic-Late Jurassic), 4) the Dio Dendra group deep-water sediments (Late Jurassic-Late Cretaceous) and 5) the underlying, Late Cretaceous-Tertiary Pindos flysch. Oligocene to Early Miocene mollasic-type sediments of the Mesohellenic trough cover the formations of the Pindos zone.

The Pindos ophiolitic nappe covers a total area of approximately 2500 km^2; it is less than 4 km thick and is tectonically emplaced over the Maastrichtian-Eocene Pindos flysch (Text-fig. 1b). Its mantle unit has a relative thickness of 3 km, whereas its cumulate sequence is only 1 km thick (Kostopoulos 1989; Rassios 1991). Although the inner parts of the complex retain a relatively coher-

ent tectono-stratigraphic structure the ophiolitic sequence itself is disrupted and can be further divided into four major tectonic units: the Dramala complex, the Loumnitsa unit and the Aspropotamos unit, all tectonically superimposed on the Avdella mélange (Jones and Robertson 1991). The mantle-cumulate Dramala imbricate represents part of the Pindos sub-oceanic mantle and its crustal cumulate sequence. The latter is in continuous section with the mantle rocks on Dramala separated by a well-pronounced 'petrological Moho' (Rassios 1991). The Dramala mantle rocks include variably depleted spinel harzburgites accompanied by minor dunites, lherzolites and plagioclase-bearing peridotites, as well as pyroxenites (Jones and Robertson 1991; Ross and Zimmerman 1996; Pelletier *et al*. 2008). As indicated by the restricted exposures of harzburgite and chert breccias that are cemented by ophicalcite, the Dramala tectonites were once exposed on the oceanic floor (Jones *et al*. 1991). The Loumnitsa unit, located at the bottom of the Dramala sequence, is thought to represent the metamorphic sole of the Pindos ophiolites. It consists of low amphibolite- to greenschist-facies metabasites, including garnet-bearing amphibolites and metasedimentary rocks (e.g., Myhill 2011) that have yielded amphibole Ar-Ar ages of 163 ± 3 and 172 ± 5 Ma (Thuizat *et al*. 1981; Spray *et al*. 1984; and references therein). The Aspropotamos crustal unit rocks cover an extremely wide range of compositional affinities, ranging from high-Ti mid-ocean ridge basalts (MORB) through types intermediate between MORB and island arc tholeiite (IAT) to IAT and younger boninite dykes (Kostopoulos 1989; Saccani and Photiades 2004; Beccaluva *et al*. 2005). U-Pb ion microprobe dating of a comagmatic zircon crystal from a gabbro specimen from the Aspropotamos unit yielded a crystallization age of $^{206}Pb/^{238}U$ at 171 ± 3 Ma, interpreted as the time of formation of the Pindos crust (Liati *et al*. 2004).

The Avdella mélange represents a subduction-accretion formation and occurs along the thrust between the Pindos ophiolitic nappe and the autochthonous Pindos flysch. It shows a chaotic structure, consisting of strongly tectonized sedimentary, magmatic and metamorphic fragments included in a sheared groundmass composed of shales and siltstones (Jones and Robertson 1991). The mélange was generally accreted because of the consumption of the Pindos oceanic lithosphere at a westward dipping suprasubduction zone (SSZ) beneath the Apulian block. The collision between the Apulian and Pelagonian continental blocks resulted in intense off-scraping and imbrication of the oceanic crust during the Late Cretaceous. The mélange was finally emplaced over the collapsed margin when the subduction trench collided with the Pelagonian margin (Danelian and Robertson 2001; Ghikas *et al*. 2010). The internal structure of the Avdella mélange is defined by thrusts developed during the collisional event (Jones and Robertson 1991).

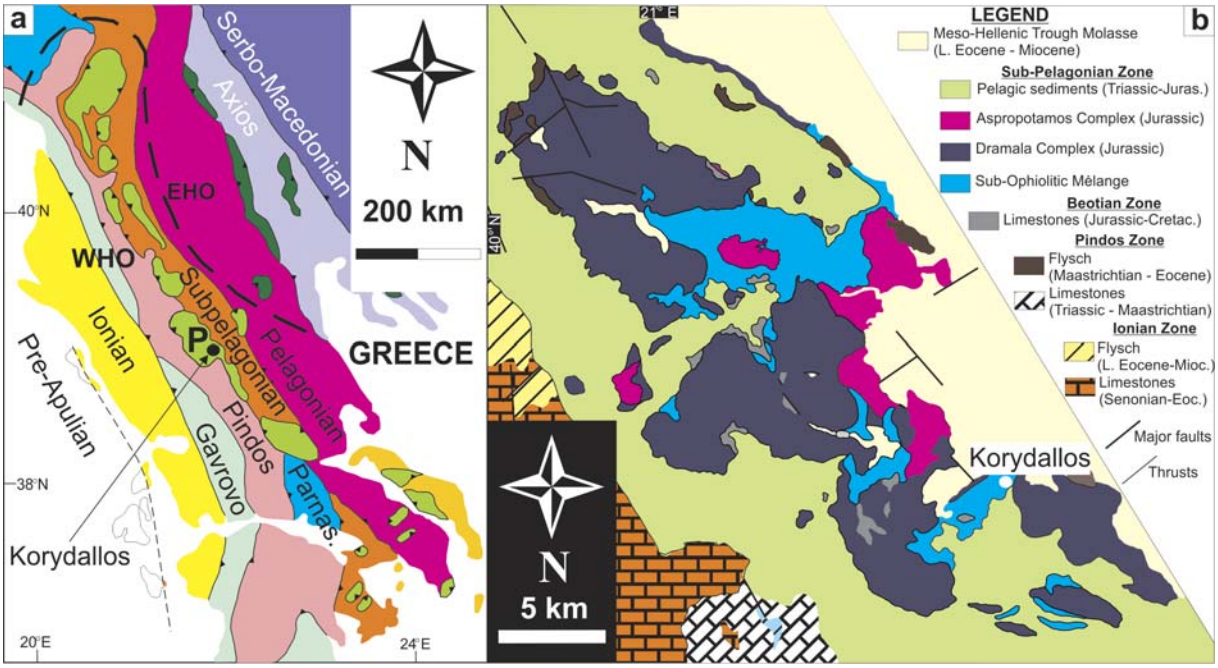

Text-fig. 1. **a** – simplified geological map of the west-central Balkan Peninsula, showing major tectonic zones and the distribution of the most extensive ophiolite outcrops. Note that the "Western Hellenic Ophiolites" (WHO) are separated from the "Eastern Hellenic Ophiolites" (EHO) by a black dashed line (P: Pindos; modified after Dilek *et al*. 2007), b – simplified geological map of the Pindos ophiolitic massif, showing the location of the study area (Korydallos district; modified after Kostopoulos 1989; Jones and Robertson 1991)

BACKGROUND INFORMATION AND RELEVANT PREVIOUS WORKS

Tarkian *et al*. (1996) and Prichard *et al*. (2008) studied the noble metal inventory of the chromitites from the district of Korydallos and the platinum-group mineral (PGM) assemblages that they host. In a similar manner Kapsiotis *et al*. (2010) and Kapsiotis (2013) focused on the geological investigation of the chromitite outcrops and explained their genesis on the basis of spinel compositions and platinum-group element (PGE) mineralogical data. A first, but short, description of the mélange formation in the Korydallos area was given by Kapsiotis (2013). According to that study the mélange in the Korydallos locality is a chaotic lithological formation consisting of a rather complex mixture of sedimentary, volcanic and plutonic tectonic blocks set in an intensely strained groundmass. The most sizeable fragment in the Korydallos mélange was proved to be composed of a serpentinite hosting two small, densely disseminated to massive, deformed chromitite pods. Based on the composition of the ore-making spinel they were classified as high-Cr and high-Al chromitites. Both chromitite occurrences are strongly affected by post-magmatic processes and their interstitial silicate matrix is completely serpentinized. An interesting petrographic feature exhibited by the refractory chromitites is that they are enriched in base metal minerals (BMM) that occur in variable textural positions within the Al-rich chromitite. These are thought to represent relics of pre-existing sulphides that have been compositionally reworked during the alteration of the high-Al chromitite pod. Another remarkable mineralogical observation was that the high-Al chromitite samples display marks of Cr-spinel replacement by an opaque spinel phase (namely ferrian chromite), whereas the same alteration type is missing from the high-Cr chromitite samples. Both chromitites are not separated by sizeable shear zones, so they retain their original positions within the serpentinite fragment. Their formation was attributed to metasomatic interaction between relatively depleted peridotites and a progressively fractionating melt with an affinity intermediate between MORB and IAT, generated in the mantle region below a small back-arc basin.

THE KORYDALLOS OPHIOLITIC MÉLANGE

A typical blocks-in-matrix mélange crops out in a 7 km by 2 km exposure located to the northeast of the village of Korydallos (Gournes district; Text-fig. 2a). This chaotic lithological formation is well developed in the area between Panagia and Pefki villages and comprises part of the Avdella mélange. It is mainly composed of a series of exotic blocks randomly scattered in a variably tectonized clastic groundmass. The fragments are metric to decametric in size and of variable morphology, including commonly unmappable lenses, sheets, slices and irregular bodies of ophiolitic and sedimentary origin. In lithological terms each fragment is composed of a single type of rock embedded in a clayish to muddy matrix. Most common are blocks of carbonate rocks including Jurassic and Upper Cretaceous pelagic limestones and fragments of ophiolitic origin. The former occur as a mappable fragment in the northernmost sector of the mélange exposure (Text-fig. 2a). Upper Cretaceous cherts may also be present but in the form of smaller exotic blocks within the matrix. Fragments of volcanic rocks are very rare, encompassing only a few slices composed of spilite or pillow lava. White to grey dolerite blocks (up to tens of m wide) stand 'proud' as isolated mounds in a low-relief groundmass. In the vicinity of such blocks the matrix appears to be relatively more fine-grained and strained. The northwestern domain of the mélange outcrop is occupied mostly by coarse-grained troctolite fragments, which can locally be more fine-grained. Due to severe serpentinization and uralitization these blocks frequently show grey to light green colors. They also bear many petrographic similarities with the adjacent massive troctolite occurrence of the Aspropotamos complex, which is tectonically emplaced on the mélange. The matrix in the western part of the mélange exposure is coarser and is composed of troctolite with minor limestone pebbles. Senses of shear are scarce and deformation in that area is expressed by stretching, giving troctolite pebbles a subrounded shape. Limited blocks of siliciclastic turbidites occur in the southern domain of the mélange exposure. Strongly serpentinized peridotites occur as mappable (Text-fig. 2a) and unmappable, rectangular bodies within the poorly sorted, serpentinite groundmass in the central and eastern domains of the mélange outcrop (Text-fig. 2a, b). The smaller peridotite fragments are dominated by yellowish, pervasively serpentinized, massive harzburgites (up to 1 m across), whereas a larger peridotite block is mainly brown to reddish, fine-grained serpentinite. The latter is about 70 m long and 50 m wide and is aligned along a NW-SE direction. It is tectonically incorporated as an imbricated thrust slice within a locally sheared groundmass, being composed mainly of non-foliated serpentinite. Some of the most striking features of this block are: i) two occurrences of small chromitite pods, ii) a series of W-E trending shear zones ranging from a few cm to 1 m in width that are not pervasive throughout the block and iii) on a local basis, stretching lineation exhibited by the accessory Cr-spinel grains. Myloniti-

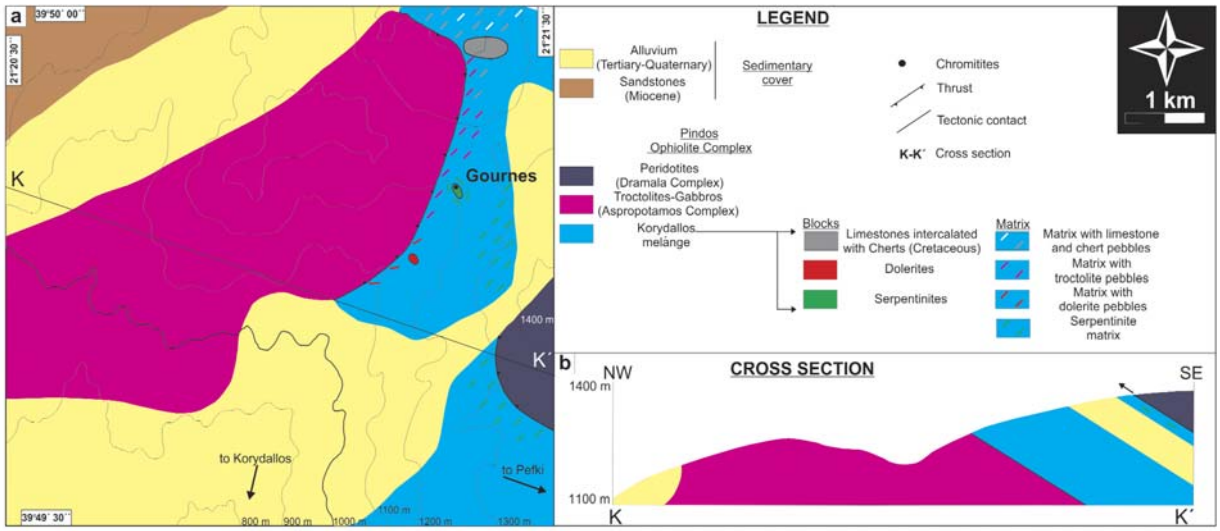

Text-fig. 2. a – Detailed geological map illustrating the distribution of the ophiolitic mélange and the location of the chromitite-bearing serpentinite block in the Korydallos district (modified after Kapsiotis *et al*. 2010), b – inset cross section representing the intersection of the different geological formations in the subsurface

zation is very common in the shear zones, although quite heterogeneous. Other deformational characteristics include open isoclinal to asymmetric folds (Text-fig. 3a) and the local development of schistosity on the boundaries between the blocks and the serpentinite matrix.

PETROGRAPHY

Serpentinite block

Serpentinites commonly exhibit mesh texture, suggesting excellent pseudomorphic substitution of serpentine for fine-grained olivine. Olivine is fully serpentinized from the edges to the core, whereas rare olivine relicts may be locally preserved as isolated 'islands' within the serpentinized groundmass, retaining evidence for ductile strain such as undulatory extinction and deformation lamellae. Sometimes the mesh cores are occupied by magnetite that also occurs as isolated, dispersed grains or as trails within the altered matrix. Chlorite is also present but is much rarer. Chlorite frequently forms small brown-colored, in cross-polarized nicols, grains disseminated in the matrix. Accessory Cr-spinel constitutes less than 2–3 vol.% of the sample and occurs as light brown, subhedral to euhedral grains that commonly exhibit deformational features such as fractures and pull-apart textures. Cr-spinel is the only primary phase that is preserved compositionally intact in the mineral assemblage of the serpentinite fragment. In a few cases magnetite was observed to be attached to Cr-spinel grains. Elongated tremolite fibers may also take part in the mineral paragenesis of the examined serpentinite block, although to a much lesser extent. Based on the pseudomorphic replacements and relict modal mineralogy it can be proposed that serpentinite was formed after complete alteration of a former spinel-bearing, fine-granoblastic textured dunite. Except for serpentinization, dunite also experienced thorough weathering, shown by the limited traces of reddish iddingsite (a complex mixture of smectite, chlorite, hematite and goethite). The results of the petrographic study are summarized in Table 1.

Chromitites

The high-Cr chromitite is densely disseminated (50–70 vol.% of Cr-spinel) to massive (70–90 vol.% of Cr-spinel), with the two different textural types being randomly distributed in the pod (Table 1). It is made up of reddish to dark brown, subhedral to euhedral magnesiochromite grains (Kapsiotis 2013) that are up to 1.5 mm in diameter. All high-Cr chromitite specimens display an irregular net of brittle fractures, which is the most profound characteristic of the impact of deformation on the chromitite (Text-fig. 3b). The interstitial silicate matrix is fully serpentinized showing mesh, and on a much rarer basis interlocking and interpenetrating, textures. The two latter are always superimposed on the first. Occasionally the mesh serpentine may be stretched, forming a ribbon texture. Sometimes the mesh cores are occupied by chlorite. Anhedral, syn-serpentinization magnetite grains may imperfectly outline the mesh rims in the densely disseminated chromitite specimens. Serpentine, chlorite and pargasite with

bornite may occur as globular or euhedral inclusions in magnesiochromite.

The Al-rich chromitite also displays densely disseminated (50–70 vol.% of Cr-spinel) to massive (70–75 vol.% of Cr-spinel) texture (Table 1). It is worthy of mention that the internal parts of the chromitite body are composed of massive Cr-spinel, whereas the outer parts are densely disseminated in texture. It is composed of light brown, subhedral to euhedral Cr-spinel grains up to 1 mm across. Cataclastic deformation is present but it is not as intense as in the Cr-rich chromitite. The interstitial groundmass is almost completely serpentinized-chloritized, exhibiting interpenetrating and interlocking texture (Text-fig. 3c). Scarce olivine relicts can still be recognized as 'islands' that have survived alteration. Chlorite is not in dispersed within the serpentine matrix but is always in textural association with Cr-spinel, exhibiting black-colored boundaries. In most samples the following replacement relationships were observed: chlorite substitutes for olivine, whereas chlorite is cross cut by serpentine (Text-fig. 3d). Randomly oriented grains and prismatic fibers of subordinate tremolite (Text-fig. 3e) are also present as secondary silicate phases, whereas abundant hydrothermally reworked BMM grains occur in a variety of textural positions that were described in detail by Kapsiotis (2013). Except for serpentine and chlorite, olivine may appear as subhedral inclusions in Cr-spinel.

Spinel textures in Al-rich chromitite

Optical investigation of the Al-rich chromitite sections revealed that several Cr-spinel grains are compositionally inhomogeneous. In particular, Cr-spinels have been replaced along grain boundaries and fractures by an opaque phase that appears to be in paragenetic association with chlorite. Careful examination of Cr-spinel grains in back scattered electron (BSE) images revealed that the opaque phase is brighter compared to the inner, intact part of the grain (Text-fig. 3f, g, h). The boundary between Cr-spinel and the opaque regions is sharp but uneven, whereas opacity is not fully developed around the Cr-spinel grains. It occurs as discontinuous, patchy and narrow (up to 250 μm) zones, typically exhibiting a porous to sieve texture. The pores have a globular to irregular shape and are filled mainly with chlorite followed by minor serpentine. In textural terms, the opaque phase is not developed as epitaxic growths over Cr-spinel grains but as a new phase that substitutes for Cr-spinel along its boundaries (Text-fig. 3f, g) and brittle fractures (Text-fig. 3h), so that the original shape of Cr-spinel crystal is preserved. Cr-spinel grains in contact with serpentine remain undamaged in both tex-

Sample numbers	Type of rock/ore	Mode of occurrence	Dominant Cr-spinel texture	Dominant silicate texture	Mineral phase percentage	Altered phases → Secondary minerals	Petrographic observations
$K_{1\text{-}6}$	Chromitite	Small and deformed pod	Massive to densely disseminated	Mesh, interlocking, interpenetrating	Cr-spn: 50-90 vol.%, Secondary silicates: 10-50 vol.%	Ol → Ser (10-50 vol.%), Chl & Mgt	Zones of cataclastic Cr-spn, Ser, Chl, Prg and BMM inclusions in Cr-spn
$G_{1\text{-}4}$	Chromitite	Small and deformed pod	Massive to densely disseminated	Interpenetrating, interlocking	Cr-spn: 70-75 vol.%, Secondary silicates: 25-30 vol.%, BMM, Ol	Ol → Ser (≤ 25 vol.%), Chl (≤ 5 vol.%), Tre Cr-spn → Fe-chr* (≤ 5 vol.%),	Incomplete Chl and Fe-chr* intergrowths, Ser, Chl and Ol inclusions in Cr-spn
$K_{7\text{-}8}$	Serpentinite (after dunite)	Sizeable exotic (weathered) block in ophiolitic mélange	Accessory subhedral to euhedral grains	Mesh (after equigranular)	Secondary silicates: 90-95 vol.%, Ol: ≤ 8 vol%, Cr-spn: 2-3 vol.%	Ol → Ser (90-95 vol.%), Chl	Relict Ol 'islands', Chl in the mesh cores

Table 1. Summary of the main petrographic features of the investigated formations from the Korydallos ophiolitic mélange. Abbreviations: Cr-spn – Cr-spinel, BMM – base metal minerals, Ol – olivine, Ser – serpentine, Chl – chlorite, Tre – tremolite, Fe-chr* – ferrian chromite (and minor magnetite), Prg – pargasite

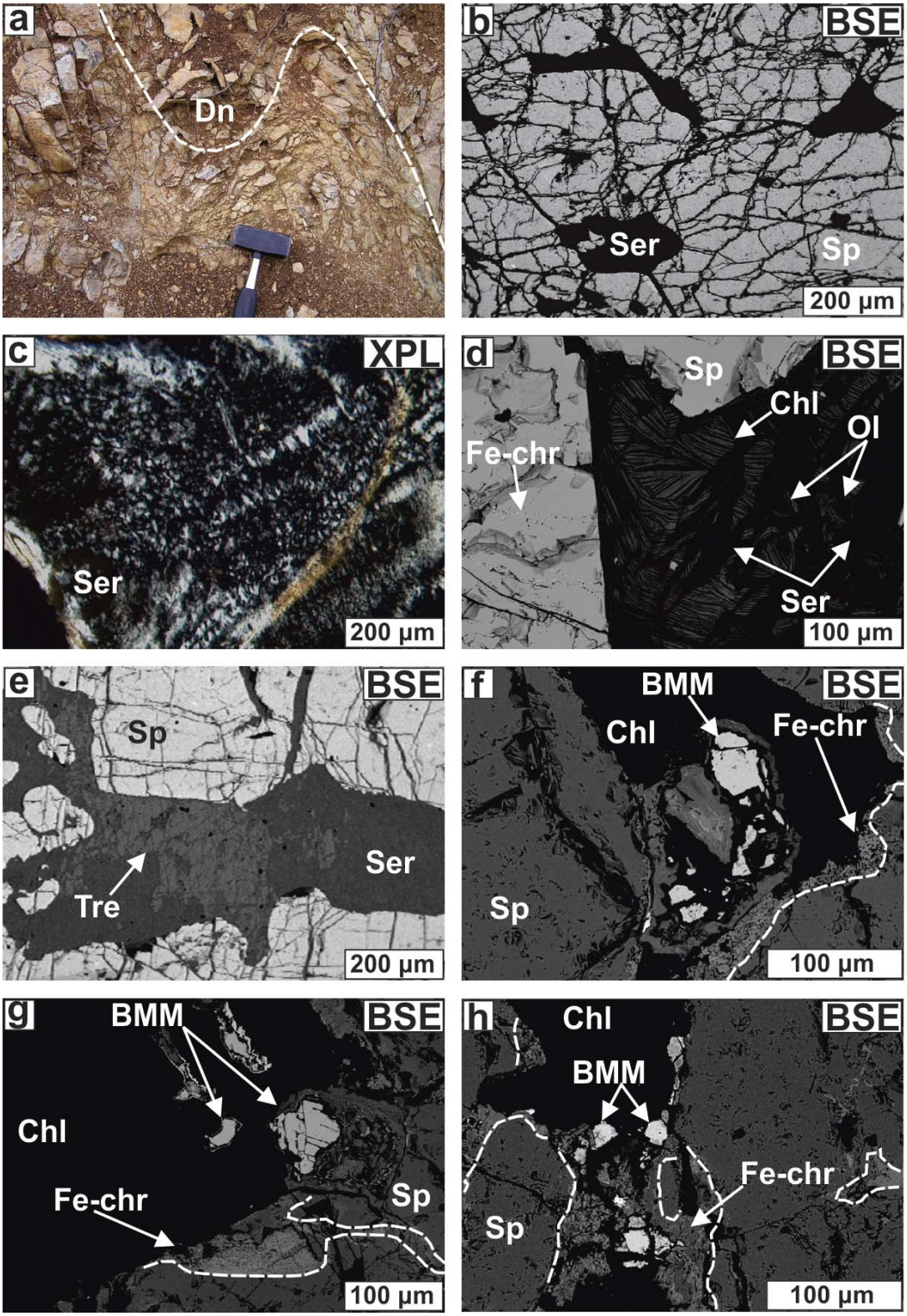

Text-fig. 3. a – folded structure in serpentinite (after dunite), b – Back Scattered Electron (BSE) image illustrating the cataclastic structure of the high-Cr chromitites, c – interlocking texture in the serpentinized matrix of the Al-rich chromitite (XPL: under cross polarized nicols), d – BSE image showing replacement of olivine by chlorite and serpentine substitution for chlorite in the high-Al chromitite, e – BSE image illustrating tremolite grains in the altered interstitial silicate groundmass of the Al-rich chromitite, f, g, h – BSE images presenting the replacement of Cr-spinel by ferrian chromite in various high-Al chromitite samples. Abbreviations: Dn - dunite, Sp - spinel, Ser - serpentine, Ol - olivine, Chl - chlorite, Fe-Chr - ferrian chromite, Tre: tremolite , BMM – base metal minerals

turally and compositionally. Compositional zoning is more frequent in densely disseminated than massive textured Al-rich chromitite samples. Although all chromitite specimens are fully serpentinized one is characterized by absence of Cr-spinel replacement by the porous, opaque phase. In addition, the extent and frequency of zoning vary substantially, even among the remaining high-Al chromitite samples.

SAMPLING AND LABORATORY METHODS

A total of ten chromitite samples were collected from two mélange-hosted, podiform chromitite bodies in the area of Korydallos. Six were from the high-Cr chromitite pod and four from the adjacent high-Al chromitite exposure. In addition, two serpentinite samples were taken from the most sizeable, chromitite-bearing, altered peridotite block in the Korydallos mélange. The studied specimens come from the Gournes district located to the north of Korydallos village. All chromitite samples were studied in terms of texture, petrography, mineral chemistry, PGE-abundances and -mineralogy by Kapsiotis (2013). In the present study the same chromitite samples, with the addition of two representative specimens from the serpentinite host, were examined mostly for alteration phenomena in Cr-spinel. Their detailed investigations revealed systematic textural-compositional zoning only in Cr-spinel grains from three Al-rich chromitite samples. Therefore, the current study is focused on their detailed examination. Analyses of intact Cr-spinel cores were presented by Kapsiotis (2013). New analytical data on the altered Cr-spinel from the high-Al chromitite, the accessory Cr-spinel of the host serpentinite and their secondary silicates are presented herein.

Cr-spinels were investigated *in situ* in polished thin sections using both conventional reflected light and electron microscopy and imaged with a Super JEOL JSM-6300 scanning electron microscope (SEM) at the University of Patras, Greece. The quantitative analyses of opaque rims, accessory Cr-spinel, serpentine, chlorite and tremolite were done using a Super JEOL JSM-6300 electron-probe micro-analyzer (EMPA) operated in wavelength-dispersive spectrometry (WDS) mode. Operating conditions were 15 kV accelerating voltage and 20 nA beam current, with a 5 μm beam diameter. The ZAF correction software was applied, whereas calibrations were performed using natural and synthetic reference materials. The proportion of ferric Fe (Fe^{3+}) in Cr-spinel was estimated assuming ideal spinel stoichiometry (AB_2O_4), whereas Ti was presumed to be present as an ulvöspinel molecule. Mn and Zn are divalent in Cr-spinel, whereas Cr valence state is +3. All Fe in silicates was taken to be ferrous (Fe^{2+}). Representative pair analyses of Cr-spinel and ferrian chromite from the investigated Al-rich chromitite and analyses of accessory Cr-spinel from serpentinite are listed in Table 2; analyses of serpentine, chlorite and tremolite are presented in Table 3.

One bulk-serpentinite sample was crushed in an achat-tungsten (W) ring mill before it was analyzed for major oxides, trace and rare earth elements (REE). Whole-rock analysis was done at ActLabs, Ontario, Canada, using a Perkin Elmer Sciex ELAN 9000 Inductively Coupled Plasma-Mass Spectrometer (ICP-MS). Analysis was performed using the analytical package '4Lithores-Lithium Metaborate/Tetraborate Fusion-ICP and ICP/MS'. The complete analytical procedure is described in detail in Hoffman (1992). Detection limits, bulk-rock major and trace element and REE concentrations are presented in Table 4.

MINERAL CHEMISTRY

Cr-spinel in serpentinite

Accessory Cr-spinels in serpentinite have a chemical composition that varies between 31.31 and 35.43 wt.% Cr_2O_3, 31.74 and 37.81 wt.% Al_2O_3, 13.98 and 15.43 wt.% MgO, 14.62 and 15.93 wt.% FeO, whereas Fe_2O_3 can be up to 4.53 wt.%. Their TiO_2 content is up to 0.47 wt.% and they do not contain any 'impurities' (e.g., SiO_2, MnO; Table 2). The Cr# [Cr/(Cr + Al)] ratio varies between 0.36 and 0.42 and Mg# [Mg/(Mg + Fe^{2+})] ranges from 0.57 to 0.62 (Text-fig. 4a, b). Such elevated Mg# values in Cr-spinels are indicative of their unaltered nature (e.g., Sobolev and Logvinova 2005). The Fe^{3+}# [Fe^{3+}/(Fe^{3+} + Cr + Al)] values are up to 0.05 (Table 2). In the Cr# vs. Mg# plot the analyzed Cr-spinel grains have compositional signatures that strongly resemble that of Cr-spinel from the enclosed high-Al chromitite pod (Kapsiotis 2013; Text-fig. 4a, b).

Opaque spinel phase

Analytical traverses across optically zoned Cr-spinels from the high-Al chromitite pod revealed detectable chemical zoning. The opaque zones across Cr-spinel boundaries and cracks exhibit the following compositional variations: 7.12 and 50.46 wt.% Cr_2O_3, 0.27 and 20.73 wt.% Al_2O_3, 0.69 and 16.52 wt.% MgO, 9.90 and 31.55 wt.% FeO, whereas Fe_2O_3 ranges between 4.09 and 57.03 wt.%, the TiO_2 content is up to

0.41 wt.% and the NiO abundance does not exceed 0.92 wt.%. SiO and MnO contents are up to 3.71 and 3.50 wt.%, respectively (Table 2). The Cr# ranges between 0.56 and 0.95 and the Mg# varies from 0.01 to 0.57 (Text-fig. 4a, b). The Fe^{3+}# values range between 0.05 and 0.88, whereas the $Fe^{3+}/(Fe^{2+} + Fe^{3+})$ ratio fluctuates between 0.14 and 0.68 (Table 2).

Kapsiotis (2013) showed that the high-Al chromitite is composed of Cr-spinel having Cr# and Mg# values that range between 0.44–0.48 and 0.59-0.64, respectively. In the Cr# vs. Mg# diagram the opaque zone analyses plot on the upper, right part, implying that they were formed after significant loss of Al_2O_3, and in most cases of MgO, from the initial Cr-spinel composition. In addition the increases in Fe^{3+}# and $Fe^{3+}/(Fe^{2+} + Fe^{3+})$ from core (≤ 0.108) to rim (0.141-0.684; Table 2) indicate that considerable oxidation of Fe^{2+} to Fe^{3+} occurred towards the external parts of Cr-spinel grains. Taking into account the composition, as well as the high reflectivity and low hardness of the opaque regions, it can be said that they vary mineralogically between a FeO^t- and Cr_2O_3-rich, Al_2O_3-poor spinel phase commonly referred to as ferrian chromite (also called 'ferritchromit' or 'ferritchromite'; Spangenberg 1943) and magnetite.

Silicates

Most serpentine grains in the high-Al chromitite specimens contain relatively elevated concentrations of Al_2O_3 (up to 2.18 wt.%), consistent with an antigorite composition. SiO_2 ranges between 41.94 and 46.67 wt.%, MgO between 37.16 and 40.64 wt.%; Cr_2O_3 may be present up to 0.34 wt.%, although is commonly below detection limits. The NiO content in serpentine is up to 1.23 wt.% (Table 3).

Chlorite in the high-Al chromitite samples has relatively elevated Cr_2O_3 abundances (up to 8.47 wt.%). The SiO_2 content varies between 27.89 and 36.04 wt.%, Al_2O_3 concentration are up to 21.81 wt.% and MgO content ranges between 31.41and 35.80 wt.%. The TiO_2, MnO and NiO contents are relatively low and commonly even below detection limits (Table 3). The Si content of chlorite allows classifying them as clinochlore after the classification proposed by Bailey (1980). Their compositional characteristics are similar to those of chlorites from other ophiolitic mantle exposures (e.g., Jan and Windley 1990).

The analyzed amphibole from the interstitial silicate groundmass of the Al-rich chromitite has an average composition corresponding to tremolite following the classification proposed by Leake *et al*. (1997). Their SiO_2 content ranges slightly from 53.01 to 54.28 wt. % and Al_2O_3 varies between 7.55 and 7.77 wt.%, in accord with Al_2O_3 abundance in metamorphic amphiboles from ophiolites (Stern and Elthon 1979). The MgO content varies between 21.68 and 22.04 wt.% and the CaO content ranges between 11.88 and 12.39 wt.%. Cr_2O_3 abundances are up to 1.85 wt.% (Table 3).

GEOCHEMISTRY OF THE SERPENTINITE BLOCK

A representative whole-rock analysis of one sample collected from the chromitite-bearing serpentinite block shows that it has high LOI value (16.19 wt.%), which is

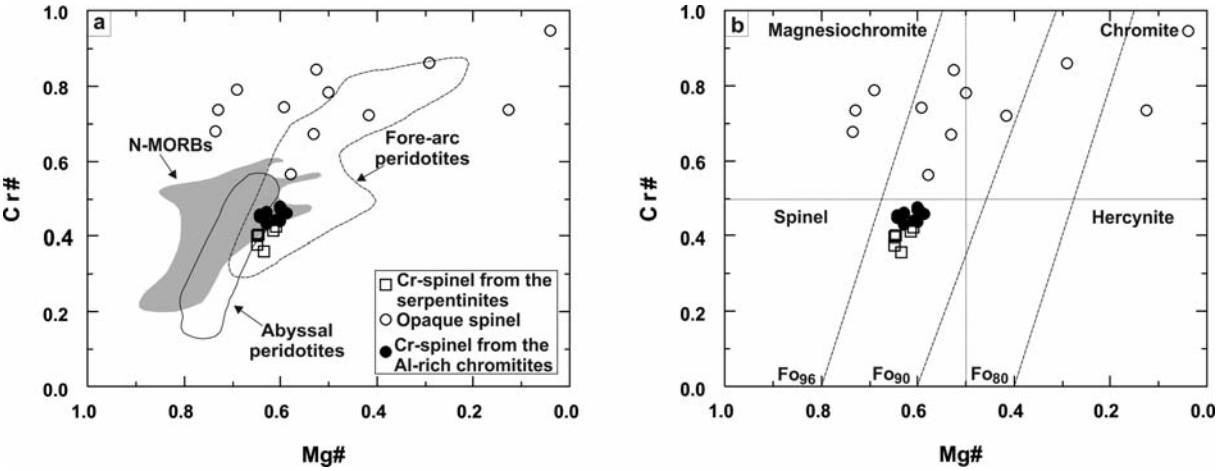

Text-fig. 4. Compositional variations of Cr-spinel cores and ferrian chromite from the high-Al chromitite and serpentinite samples in terms of: a – Cr# [Cr/(Cr + Al)] versus Mg# [Mg/(Mg + Fe^{2+})]. Data for spinel in modern abyssal peridotites are from Dick and Bullen (1984) and Juteau *et al*. (1990). Field for spinel in equilibrium with N-MORB's is taken from Dick and Bullen (1984). Data for spinel in fore-arc peridotites are from Ishii *et al*. (1992) and Ohara and Ishii (1998), b – Classification of the composition of Cr-spinel and ferrian chromite from the peridotites in terms of Cr# vs. Mg#. Cr-spinel composition is also contoured at a nominal temperature of 1200 °C for olivine compositions from Fo_{80} to Fo_{96} (quantitatively computed by Dick and Bullen 1984)

Lithology	High-Al chromitite													
Sample	G_2	G_2	G_2	G_2	G_2	G_2	G_3	G_3	G_3	G_3	G_3	G_3	G_3	G_3
Analysis	1	1_a	2	2_a	3	3_a	5	5_a	6	6_a	10	10_a	11	11_a
SiO_2 (wt.%)	-	-	-	1.49	-	0.53	-	-	-	-	-	2.00	-	2.75
TiO_2	0.21	0.35	0.36	-	0.20	0.26	0.17	0.30	0.29	-	0.29	0.41	0.26	-
Al_2O_3	26.10	14.50	32.29	0.27	30.12	10.56	29.69	6.30	30.22	20.73	31.70	12.63	31.97	10.79
Cr_2O_3	43.58	43.70	36.13	7.12	38.83	43.79	38.81	50.46	39.96	39.50	38.13	48.31	37.19	44.86
Fe_2O_3	0.09	12.92	2.03	57.03	2.05	12.64	1.30	16.45	0.19	11.66	1.07	4.09	-	12.14
FeO	16.99	17.48	15.42	31.55	15.14	27.97	16.04	17.04	16.30	15.99	14.62	22.50	16.06	10.96
MnO	0.14	-	-	-	0.10	3.50	0.51	-	-	0.65	0.02	0.37	0.02	0.43
MgO	12.50	11.13	14.57	0.69	14.37	2.27	13.24	10.56	13.74	12.27	14.86	9.00	13.62	16.52
NiO	-	-	-	-	-	-	-	0.38	-	-	0.24	0.19	-	-
Total	99.61	100.08	100.80	98.15	100.81	101.52	99.76	101.49	100.70	100.80	100.93	99.50	99.12	98.45
Cations calculated on the basis of 8 atoms of O														
Si	-	-	-	0.057	-	0.018	-	-	-	-	-	0.066	-	0.088
Ti	0.005	0.009	0.008	-	0.004	0.007	0.004	0.007	0.006	-	0.006	0.010	0.006	-
Al	0.938	0.552	1.108	0.012	1.043	0.429	1.046	0.247	1.051	0.758	1.087	0.490	1.119	0.405
Cr	1.050	1.117	0.832	0.217	0.902	1.193	0.917	1.327	0.932	0.969	0.877	1.257	0.873	1.129
Fe^{3+}	0.002	0.314	0.045	1.656	0.045	0.328	0.029	0.412	0.004	0.272	0.024	0.101	-	0.291
Fe^{2+}	0.433	0.472	0.375	1.018	0.372	0.806	0.401	0.474	0.402	0.415	0.356	0.619	0.399	0.292
Mn	0.004	-	-	-	0.002	0.102	0.013	-	-	0.017	-	0.01	0.001	0.012
Mg	0.568	0.536	0.632	0.040	0.630	0.117	0.590	0.524	0.604	0.568	0.644	0.442	0.603	0.784
Ni	-	-	-		-	-	-	0.010	-	-	0.006	0.005	-	-
Σ	3.000	3.000	3.000	3.000	2.998	3.000	3.000	3.001	2.999	2.999	3.000	3.000	3.001	3.001
Cr#	0.53	0.67	0.43	0.95	0.46	0.74	0.47	0.84	0.47	0.56	0.45	0.72	0.44	0.74
Mg#	0.57	0.41	0.60	0.01	0.60	0.09	0.58	0.37	0.60	0.45	0.63	0.38	0.60	0.57
Fe^{3+}#	0.001	0.158	0.023	0.879	0.023	0.168	0.015	0.207	0.009	0.136	0.012	0.055	-	0.159
$Fe^{3+}/(Fe^{2+} + Fe^{3+})$	0.005	0.399	0.106	0.619	0.108	0.289	0.068	0.465	0.010	0.396	0.062	0.141	-	0.499

Table 2. Representative electron-microprobe analyses of Cr-spinel and ferrian chromite pairs and Cr-spinel cores from the high-Al chromitite and serpentinite samples, respectively [Cr#: Cr/(Cr + Al), Mg#: Mg/(Mg + Fe^{2+}), Fe^{3+}#: $Fe^{3+}/(Fe^{3+} + Cr + Al)$, – : below detection limit]. Cr-spinel core analyses from the Al-rich chromitite are taken from Kapsiotis (2013)

Lithology	High-Al chromitites						Serpentinite (after dunite)					
Sample	G_4	G_4	G_4	G_4	G_4	G_4	K_7	K_7	K_7	K_7	K_7	K_7
Analysis	1	1_a	2	2_a	3	3_a	1	2	3	4	5	6
SiO_2 (wt.%)	-	3.71	-	-	-	0.02	-	-	-	-	-	-
TiO_2	0.14	-	0.17	0.04	0.20	-	0.29	0.06	0.47	0.26	0.29	0.31
Al_2O_3	30.06	7.87	31.85	12.51	30.34	7.65	37.81	33.66	35.89	33.74	31.74	34.21
Cr_2O_3	37.86	42.08	37.58	39.01	38.39	42.13	31.31	33.01	32.39	35.43	34.76	34.3
Fe_2O_3	1.93	12.54	-	23.81	0.54	26.69	0.84	4.53	2.07	-	3.42	2.07
FeO	14.57	19.62	15.55	9.90	16.48	11.62	15.50	14.62	14.87	15.64	15.93	14.87
MnO	0.71	0.80	0.54	0.54	-	-	-	-	-	-	-	-
MgO	13.94	10.95	13.57	15.38	13.15	14.44	15.06	15.06	15.43	14.02	13.98	15.11
NiO	0.06	-	0.10	0.18	0.21	-	-	-	-	-	-	-
Total	99.27	97.57	99.36	101.37	99.31	102.55	100.81	100.94	101.12	99.09	100.12	100.87
Cations calculated on the basis of 8 atoms of O												
Si	-	0.125	-	-	-	0.001	-	-	-	-	-	-
Ti	0.003	-	0.004	0.001	0.005	-	0.006	0.001	0.010	0.006	0.006	0.007
Al	1.057	0.312	1.113	0.464	1.070	0.289	1.266	1.145	1.206	1.170	1.102	1.161
Cr	0.893	1.120	0.881	0.970	0.909	1.067	0.703	0.754	0.730	0.824	0.810	0.781
Fe^{3+}	0.043	0.318	-	0.564	0.012	0.643	0.018	0.098	0.044	-	0.076	0.045
Fe^{2+}	0.364	0.552	0.386	0.260	0.413	0.311	0.368	0.353	0.354	0.385	0.392	0.358
Mn	0.018	0.023	0.014	0.014	-	-	-	-	-	-	-	-
Mg	0.620	0.550	0.600	0.722	0.587	0.689	0.638	0.648	0.656	0.615	0.614	0.649
Ni	0.001	-	0.002	0.005	0.005	-	-	-	-	-	-	-
Σ	2.999	3.000	3.000	3.000	3.001	3.000	2.999	2.999	3.000	3.000	3.000	3.001
Cr#	0.46	0.78	0.44	0.68	0.46	0.79	0.36	0.40	0.38	0.41	0.42	0.40
Mg#	0.60	0.39	0.61	0.47	0.58	0.42	0.62	0.59	0.62	0.62	0.57	0.62
Fe^{3+}#	0.022	0.182	-	0.282	0.006	0.322	0.009	0.049	0.022	-	0.038	0.023
$Fe^{3+}/(Fe^{2+} + Fe^{3+})$	0.107	0.365	-	0.684	0.029	0.674	0.046	0.218	0.111	-	0.162	0.111

Table 2. (Continue) Representative electron-microprobe analyses of Cr-spinel and ferrian chromite pairs and Cr-spinel cores from the high-Al chromitite and serpentinite samples, respectively [Cr#: Cr/(Cr + Al), Mg#: Mg/(Mg + Fe^{2+}), Fe^{3+}#: $Fe^{3+}/(Fe^{3+} + Cr + Al)$, – : below detection limit]. Cr-spinel core analyses from the Al-rich chromitite are taken from Kapsiotis (2013)

Table 3. Representative electron-microprobe analyses of serpentine from the high-Al chromitite and serpentinite samples, and of chlorite and tremolite from the Al-rich chromitite (–: below detection limit)

Lithology	High-Al chromitite				Serpentinite (after dunite)	High-Al chromitite								High-Al chromitite			
Mineral	Serpentine					Chlorite								Tremolite			
Sample	G_2	G_2	G_3	G_3	K_7	K_7	G_2	G_2	G_3	G_3	G_3	G_4	G_4	G_2	G_3	G_3	G_4
Analysis	1	2	3	4	2	3	1	2	3	4	5	6	7	8	9	1	2	1
SiO_2 (wt.%)	41.94	44.43	46.21	46.67	39.70	38.29	36.04	33.07	33.59	27.89	33.2	33.1	34.60	32.69	35.91	53.22	53.01	54.28	54.01
TiO_2	-	-	-	0.09	0.11	-	-	-	0.17	-	0.15	-	-	0.65	0.57	-	-	-	-
Al_2O_3	2.18	0.73	0.98	0.73	0.53	0.59	15.92	19.36	13.59	12.59	15.74	21.81	14.35	16.36	19.77	7.64	7.77	7.55	7.61
Cr_2O_3	0.34	-	-	-	-	-	0.55	2.30	3.90	8.47	4.34	1.36	1.80	1.28	0.41	1.85	1.76	1.24	1.44
$Fe_2O_3^t$	4.41	1.67	1.83	2.52	5.04	5.92	0.85	2.10	2.33	4.21	1.60	2.57	5.94	2.77	1.26	1.63	1.72	1.67	1.55
MgO	37.26	37.91	40.64	40.12	39.29	38.12	35.8	34.38	33.47	31.41	35.10	33.98	34.55	33.17	34.78	22.04	21.91	21.68	21.71
NiO	1.23	0.73	1.12	0.54	0.26	-	-	-	0.37	0.51	0.30	0.56	-	0.33	-	-	-	-	-
MnO	-	-	0.18	0.22	-	-	-	-	-	-	-	0.20	0.05	0.40	0.33	-	-	-	-
CaO	-	-	-	-	-	-	-	-	-	-	-	-	-	-	-	11.88	12.09	12.24	12.39
Na_2O	-	-	-	-	-	-	-	-	-	-	-	-	-	-	-	0.96	0.88	0.75	0.69
K_2O	-	-	-	-	-	0.13	-	-	-	-	-	-	-	-	-	0.45	0.51	-	-
Total	87.36	85.47	90.96	90.89	84.93	83.05	89.16	91.21	87.42	85.08	90.43	93.58	91.29	87.65	93.03	99.67	99.65	99.41	99.40
	Cations calculated on the basis of 9 atoms of O						Cations calculated on the basis of 28 atoms of O									Cations calculated on the basis of 23 atoms of O			
Si	1.962	2.085	2.049	2.067	1.917	1.898	6.512	5.931	6.345	5.625	6.056	5.799	6.323	6.136	6.233	7.187	7.169	7.304	7.274
Al^{IV}	0.038	0.005	0.001	0.003	0.033	0.034	1.488	2.069	1.655	2.375	1.944	2.201	1.677	1.864	1.767	0.813	0.831	0.696	0.726
Al^{VI}	0.082	0.040	0.051	0.038	-	-	1.900	2.020	1.368	0.615	1.437	2.299	1.411	1.752	2.274	0.403	0.407	0.501	0.481
Ti	-	-	-	0.003	0.004	-	-	-	0.024	-	0.021	-	-	0.092	0.074	-	-	-	-
Cr	0.013	-	-	-	-	-	0.078	0.326	0.582	1.349	0.625	0.188	0.260	0.19	0.056	0.198	0.188	0.132	0.153
Fe^{+3}	0.160	0.060	0.060	0.080	0.180	0.220	-	-	-	-	-	-	-	-	-	-	-	-	-
Fe^{+2}	-	-	-	-	-	-	0.128	0.315	0.368	0.710	0.244	0.377	0.908	0.435	0.183	0.184	0.194	0.188	0.175
Ni	0.050	0.030	0.040	0.020	0.010	-	-	-	0.060	0.080	0.040	0.080	-	0.050	-	-	-	-	-
Mn	-	-	0.007	0.008	-	-	-	-	-	-	-	0.030	0.008	0.064	0.049	-	-	-	-
Mg	2.598	2.652	2.687	2.649	2.828	2.817	9.643	9.193	9.425	9.443	9.544	8.875	9.412	9.282	9.000	4.437	4.417	4.349	4.359
Ca	-	-	-	-	-	-	-	-	-	-	-	-	-	-	-	1.719	1.752	1.764	1.788
Na	-	-	-	-	-	-	-	-	-	-	-	-	-	-	-	0.251	0.231	0.196	0.180
K	-	-	-	-	-	0.008	-	-	-	-	-	-	-	-	-	0.078	0.088	-	-
Σ	4.900	4.870	4.900	4.870	4.970	4.980	19.749	19.854	19.827	20.197	19.911	19.849	19.999	19.865		15.270	15.277	15.130	15.136

indicative of strong alteration of the peridotite. The serpentinite sample is strongly depleted in fusible major oxides (Al_2O_3: 0.66 wt.%, CaO: 0.12 wt.%; Na_2O: 0.08 wt.%; TiO_2: 0.007 wt.%) and trace elements (Sc: 4 ppm and V: below detection limits). In addition, it is enriched in transition elements (Cr: 2780 ppm and Ni: 2110 ppm). The REE content of the serpentinite sample is very low (0.069 ppm) and is worthy of note that except for Sm only the heaviest REE (HREE) were measured, whereas the other REE were lower than the detection limits (Table 4). Their low Nb (0.4 ppm) and Ti abundances coincide with their relative enrichment in Hf (0.3 ppm) and Zr (14 ppm) and their high Cr concentration and elevated Mg# (91.3). The serpentinite sample falls slightly above the terrestrial melting array in the Al_2O_3/SiO_2 vs. MgO/SiO_2 plot (not shown here), implying that MgO was not lost due to sea-floor weathering (Snow and Dick 1995) or conversely addition of MgO through mantle metasomatism. The CIPW normative mineralogy calculation indicates that the sample represents a former dunite (Table 4) in accordance with the assumption made from the pseudomorphic replacements.

DISCUSSION

Derivation of the peridotite block and its incorporation into the Avdella mélange

The chromitite-bearing serpentinite block exhibits a fine-mesh serpentine texture, which is thought to result from almost complete replacement of equigranular olivine by serpentine. Judging from the deformed nature of the few relict olivine grains it can be said that the studied tectonic clast was affected by intracrystalline mantle strain prior to serpentinization. Generally, fine-grained, equigranular peridotite microstructures are thought to be formed under conditions of elevated stress (pressure higher than 10 MPa) and relatively low temperature (below 1000 °C; Nicolas 1986, 1989; Ceuleneer *et al*. 1988). Such microtextures of 'lithospheric' origin probably represent increased tectonic stress and strain rate deformation of the sub-oceanic mantle (Dijkstra *et al*. 2003). On the other hand, other structural features such as mylonitic shear zones and folds (Text-fig. 3a) are interpreted to be a result of strain linked to the ductile to brittle deformation boundary (around 700 °C; Nicolas 1989). Thus, the majority of the textural-structural data suggest pre-serpentinization, deformation flow of a former dunite under conditions of relatively high pressure at a temperature interval between 700 and 1000 °C, which are typical of lithospheric mantle deformation (Suhr 1993).

The chemical composition of accessory Cr-spinel grains in the serpentinite fragment can be used to extract information on the geodynamic environment in which the initial peridotite was formed. It is generally

Lithology	Serpentinite (after dunite)	Detection limits
Sample	K_7	4Lithores
SiO_2 (wt.%)	33.44	0.01
TiO_2	0.007	0.001
Al_2O_3	0.66	0.01
Fe_2O_{3t}	7.92	0.01
MnO	0.105	0.001
MgO	42.11	0.01
CaO	0.12	0.01
Na_2O	0.08	0.01
K_2O	-	0.01
P_2O_5	-	0.01
LOI	16.19	0.01
Total	100.60	
Mg#	91.30	
Cr (ppm)	2780	20
Co	110	1
Ni	2110	20
Zn	40	30
Zr	14	1
Nb	0.4	0.2
Ba	3	3
Sc	4	1
Ga	1	1
Th	0.09	0.05
Ta	0.05	0.01
Hf	0.3	0.1
Ge	0.7	0.5
U	0.03	0.01
La (ppm)	-	0.05
Ce	-	0.05
Pr	-	0.01
Nd	-	0.05
Sm	0.001	0.01
Eu	-	0.005
Gd	-	0.01
Tb	-	0.01
Dy	-	0.01
Ho	-	0.01
Er	0.003	0.01
Tm	0.005	0.005
Yb	0.05	0.01
Lu	0.01	0.002
Cpx (CIPW)	0.57	
Opx	-	
Ol	99.43	

Table 4. Whole-rock major oxides (wt.%), trace elements, REE concentrations (ppm) and CIPW proportions in the serpentinite specimen [Mg#: MgO/(MgO + FeO), –: below detection limit]

accepted that Cr-spinels with high Cr# (> 0.60) and relatively low TiO_2 abundances occur in peridotites that come from arc-related settings, whereas Cr-spinels displaying lower Cr# values (< 0.60) and higher TiO_2 concentrations are contained in peridotites related to spreading regimes (e.g., Dick and Bullen 1984; Juteau *et al*. 1990; Ishii *et al*. 1992; Ohara and Ishii 1998). On the Cr# vs. Mg# plot the Cr-spinels from the studied exotic fragment fall on the boundaries between the fields of spinels from fore-arc and modern abyssal peridotites (Text-fig. 4a). Moreover, on the TiO_2 vs. Al_2O_3 diagram Cr-spinel analyses plot within the overlap area between spinels from back arc basin basalts (BABB) and MORBs as well as within the intersection of the fields representing the composition of spinel from SSZ- and MORB-type peridotites (Text-fig. 5). Overall the compositional data indicate that Cr-spinels with such chemical signatures can be found in peridotites from the mantle wedge above a subducted slab. However, they cannot originate from fore-arc to purely arc-type peridotites, because of their low Cr#. Taking into account the subhedral to euhedral crystal shape and the elevated TiO_2 abundances of the accessory Cr-spinels in serpentinite it can be claimed that they do not represent residual Cr-spinels. Their low Cr# values combined with their high TiO_2 contents are suggestive of Cr-spinels from mantle peridotites in fast-spreading back-arc basins (e.g., Ohara *et al*. 2002; Ohara 2006). Plausibly they have formed as the result of metasomatic interaction of the former peridotite with an invading mafic melt. A similar origin has been proposed by Kapsiotis (2013) for the chromitites of Korydallos based on spinel compositions, and by Pelletier *et al*. (2008) for the Dramala spinel-bearing harzburgites on the basis of their B, Li and Be whole-rock and primary mineral abundances.

In geochemical terms, although one sample cannot build a statistically robust dataset, the small size of the investigated serpentinite block combined with its consistent mineralogy may allow a preliminary assumption with respect to its derivation. Its bulk-rock analysis revealed its strongly depleted nature in major and trace magmaphile elements, and in REE. On the other hand, serpentinite is enriched in compatible elements such as Ni and Cr and in incompatible substances as Hf and Zr, displaying an elevated Mg# value (91.3). Therefore, it can be claimed that such geochemical signatures are reminiscent of SSZ-type, refractory peridotites (Text-fig. 6) from other depleted mantle exposures elsewere (e.g., Marianna back-arc basin, Ohara *et al*. 2002; Yarlung-Zangbo ophiolite, Dubois-Coté *et al*. 2005).

Consequently, it can be deduced that the serpentinite body was tectonically emplaced as an upper mantle slice of back-arc origin in an accretionary prism that was intensely reworked during the Alpine orogeny. Hence, the ultramafic component of the Korydallos mélange represents tectonic slices of a dismembered oceanic basement that evolved between the Apulia and Pelagonian microcontinents in the early Mesozoic. This interpretation is in accordance with the common consensus that the Pindos oceanic lithosphere, within the northwestern branch of the Neotethys, was located in an intra-oceanic subduction zone subsequent to its formation (e.g., Saccani and Photiades 2004; Saccani *et al*. 2011) and prior to its partial incorporation into the Avdella sub-ophiolitic mélange (Jones and Robertson 1991).

Origin of Cr-spinel alteration

Although all the high-Al chromitite samples are fully serpentinized the frequency of Cr-spinel alteration varies significantly from specimen to specimen. Considerable variations were also observed even within single chromitite samples since only a minority of the ore-making Cr-spinel grains exhibit signs of alteration. It was observed that densely disseminated textured samples are composed of Cr-spinels exhibiting stronger alteration than massive textured types. In contrast, one completely serpentinized, massive Al-rich chromitite sample was found to be entirely devoid of any Cr-spinel alteration effects. In addition, it was observed that Cr-spinels in the surrounding serpentinite and the adjacent Cr-rich chromitite pod are unaffected by alteration. Such remarks indicate that metamorphism rather than serpentinization controls Cr-spinel modification and that the Cr-spinel to silicate ratio governs the extent of that process. Microtextural features such as clinochlore substitution for olivine and subsequent clinochlore disruption by serpentine imply that metamorphism post-dates mantle processes, whereas it essentially pre-dates serpentinization (e.g., Grieco and Merlini 2011).

The discontinuous and restricted development of ferrian chromite along Cr-spinel grain boundaries and fracture walls suggests that post-magmatic alteration has not taken place uniformly and follows no clear crystallographic orientation (e.g., Mukherjee *et al*. 2010). Moreover, the textural immaturity of the ferrian chromite stresses the establishment of low P_{H_2O} conditions during Cr-spinel alteration (Candia and Gaspar 1997) in the context of a rather brief, retrograde metamorphic event (e.g., Saumur and Hattori 2013). In the course of this metamorphic episode minor Cr-spinel replacement by ferrian chromite took place due to

clinochlore substitution for olivine. Cr-spinel lost components such as Al_2O_3 and MgO that were partitioned into clinochlore, whereas it became enriched residually in Cr_2O_3 and FeO^t thus forming ferrian chromite. Such elemental exchanges are driven by the subsequent dissolution-precipitation reaction, given by Gervilla *et al*. (2012): $4(Mg_{0.7}Fe_{0.3})CrAlO_4 + 4Mg_2SiO_4 + 2SiO_{2(aq.)} + 8H_2O \rightarrow 2Mg_5AlSi_3AlO_{10}(OH)_8 + 2(Fe_{0.6}Mg_{0.4})Cr_2O_4$.

Although the ferrian chromite is texturally immature, its composition is characterized by significant variations. For instance, it displays a wide range of Fe^{3+}#

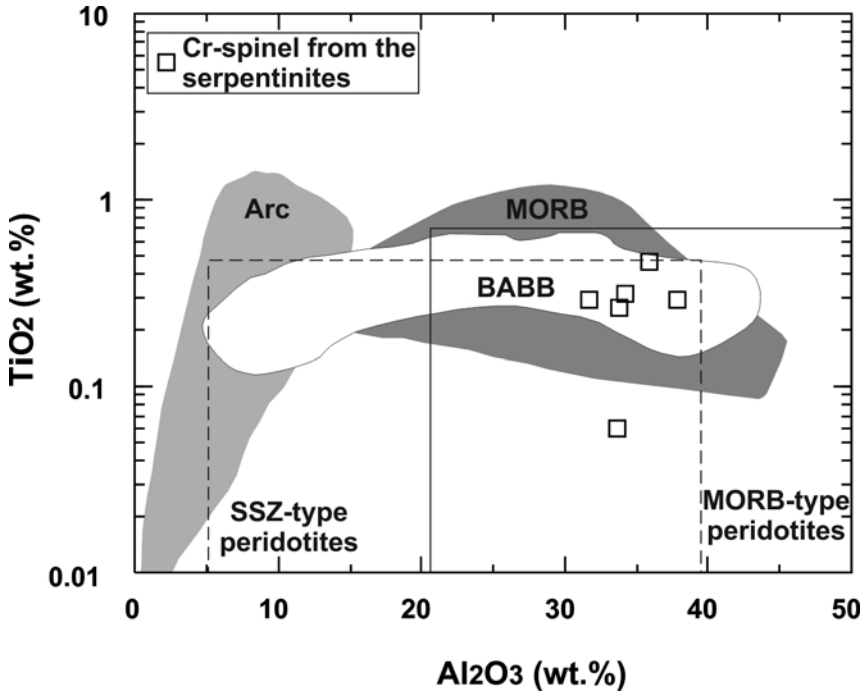

Text-fig. 5. Compositional variations of Cr-spinel cores from the studied serpentinite block in terms of TiO_2 vs. Al_2O_3. Data for spinel in BABB, MORB, MORB- and SSZ-type peridotites are from Kamenetsky *et al*. (2001)

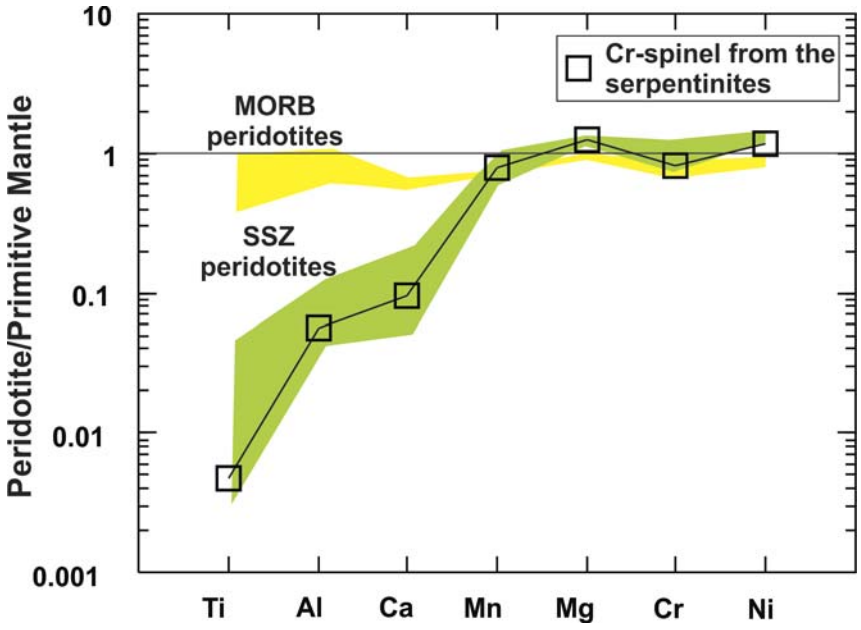

Text-fig. 6. Primitive mantle normalized pattern of whole-rock data from the serpentinite block in the mélange of Korydallos. The compatibility of elements increases from Ti towards Ni. Fields for MORB- and SSZ-type peridotites are from Sun and Nesbitt (1977)

values (0.05-0.32), which implies considerable discrepancies in the oxidation conditions during the alteration process, varying from low to moderately oxidizing. Therefore, it can be inferred that although the metamorphic incident responsible for Cr-spinel alteration was short-lived, it was quite intense to allow the formation of compositionally mature ferrian chromite (e.g., Kapsiotis 2014).

Nevertheless, in addition to ferrian chromite, magnetite was also found as a minor alteration product of Cr-spinel in the high-Al chromitite pod. It has been proposed that a pre-existing network of interconnected pores in porous ferrian chromite can dissolve clinochlore in the voids, hence stimulating diffusion of Fe^{2+} and Fe^{3+} into ferrian chromite, according to the reaction: $(Fe_{0.6}Mg_{0.4})Cr_2O_4 + Fe_3O_4 \rightarrow 2(Fe_{0.8}Mg_{0.2})CrFeO_4$ (Gervilla *et al*. 2012).

The amount of magnetite in chromitite was only limited because of the low volume of the pore system in ferrian chromite (e.g., Colás *et al*. 2012). Such a replacement may account for the coincidental concomitance of metamorphic magnetite with ferrian chromite in the Al-rich chromitite.

Cr-spinel cores are commonly characterized by considerably lower contents of SiO_2 and MnO with respect to altered regions. According to several studies the elevated SiO_2 abundances in spinel represent impurities that may be due to the presence of minor secondary silicate phases (serpentine and chlorite) as intergrowths or micro-inclusions within altered spinel (e.g., Mellini *et al*. 2005; Derbyshire *et al*. 2013). On the other hand, MnO contents over 0.50 wt.% are rare in spinels (e.g, Barnes 2000; Ahmed *et al*. 2001; Gahlan and Arai 2007). The secondary silicate minerals in the Korydallos high-Al chromitite do not contain significant MnO abundances, hence the source of Mn should be external (e.g., Grieco and Merlini 2011). According to theoretical predictions Mn is more susceptible to leaching by weakly acid solutions (e.g., Stanton 1972). The possible circulation of such a Mn-bearing fluid in the chromitite was largely facilitated by the net of brittle fractures developed on Cr-spinel grains.

Post-magmatic evolution and conditions of metamorphism

Combined textural and compositional data indicate that metamorphic alteration took place in two main stages, probably after a previous stage of subsolidus equilibration between Cr-spinel and pre-existing olivine containing approximately Fo_{93}, since Cr-spinel core compositions run between the Fo_{90} and Fo_{96} contours (Text-fig. 4b). The first metamorphic imprint is related to olivine alteration to clinochlore, probably under hydrous conditions and decreasing SiO_2 activity (Colás *et al*. 2012). Evidence of such high H_2O and SiO_2 activities in the post-magmatic fluid can be found in the relative abundance of tremolite grains and fibers scattered in the silicate groundmass of the Al-rich chromitite body. During that stage replacement of Cr-spinel by ferrian chromite (and minor magnetite) occurred under variably oxidizing conditions, as is suggested by the increasing values of the $Fe^{3+}/(Fe^{3+} + Fe^{+2})$ ratio from grain cores to boundaries. In addition, Cr-spinel alteration should have taken place in equilibrium with a significantly different olivine composition since the alteration trend runs outside the Fo_{80} and Fo_{96} contours. However, this must be due to olivine replacement by clinochlore. The second stage of post-magmatic evolution is linked to pervasive serpentinization of the silicate matrix in both chromitite pods and surrounding dunite, probably as a result of the mantle's exposure to the ocean-floor and consequent alteration prior to thrusting.

On the ternary Cr-Al-Fe^{3+} diagram Cr-spinel analyses plot within the compositional field of primary spinel from mantle chromitites (Text-fig. 7). On the other hand, ferrian chromite analyses plot mostly within the field of spinel compositions that correspond to low-amphibolite facies metamorphism. Additionally, one analysis plots in the field of metamorphic magnetite. Phase relations in the system $(Fe^{2+},Mg)Cr_2O_4$ - $(Fe^{2+},Mg)Fe^{3+}{}_2O_4$ - $(Fe^{2+},Mg)Al_2O_4$ suggest that the alteration of Cr-spinel could have taken place at temperatures close to 600 °C, evolving down to temperatures lower than 500 °C. Such a temperature interval is in accordance with the formation of clinochlore and serpentine. In particular, the formation of clinochlore provides an upper thermal limit at 700–800 °C (for depths between 10–40 km; Pawley 2002) for the first stage of metamorphic alteration, whereas the presence of pseudomorphic (mesh) serpentine gives a lower limit between 200–300 °C for the second post-magmatic event (e.g., Ernst 1993; Bach *et al*. 2006; Merlini *et al*. 2009; Grieco and Merlini 2011). The proposed decrease in temperature from approximately 700 °C to 300–200 °C delineates the transition from low-grade amphibolite to greenschist facies as a result of retrograde metamorphism during exhumation.

Evidence for a high-T post-magmatic fluid

One of the most intriguing observations made in the present study was the absence of any signs of alteration of the accessory Cr-spinel in the serpentinite and the

ore-making magnesiochromite of the high-Cr chromitite, although alteration is notable in Cr-spinel from the adjacent high-Al chromitite. This is quite unusual taking into account the small size of the chromitite-bearing serpentinite block. Generally, it seems that the impact of alteration was greater in the chromitites compared to the host serpentinite as it is confirmed from the exclusive presence of pseudomorphic serpentine in the latter. In addition, it is peculiar that even though the chromitites occur in close proximity, they display remarkable textural and mineralogical differences in terms of post-magmatic processes.

Kapsiotis (2013) showed that the high-Cr chromitite pod is composed of magnesiochromite, whereas the high-Al chromitite of Cr-spinel. It is known that magnesiochromite belongs to the category of the so-called 'normal' spinels, whereas Cr-spinel is thought to be of 'inverse' structure (Hill *et al*. 1979; Wood *et al*. 1986). According to Burkhard (1993) the latter are more susceptible to alteration, thus l structural differences may explain the discrepancies in alteration effects. However, such an assumption is applicable only to pure end-members. Another possible scenario for the absence of alteration in magnesiochromite from the Cr-rich chromitite involves the prolonged deformation of the high-Al chromitite under lithospheric (ductile) to crustal (brittle) conditions. Nevertheless, this does not seem to be the case since the latter do not occur within shear zones and they exhibit cataclastic fractures to a lesser extent than the former. Therefore, deformation can account for the alteration variations. In addition, although limited mylonitic zones were observed in the peridotite block they were not found to affect compositionally the accessory Cr-spinels in serpentinite. Furthermore, time can be a very important prerequisite that governs the progress of metamorphism. For instance, metamorphic fluids could have the opportunity to interact with the high-Al chromitite for a more extended period of time compared to the Cr-rich chromitite. Still the close proximity of the two chromitite pods is a restrictive factor for any variations in the duration of the metamorphic impact on each chromitite.

Kapsiotis (2013) proposed that the chromitites from the Korydallos area crystallized from a progressively differentiating MORB/IAT melt, first precipitating the high-Cr chromitite and then the BMM-bearing, high-Al chromitite. The appearance of high temperature, secondary silicate phases such as tremolite and clinochlore in the interstitial matrix of the Al-rich chromitite indicates that H_2O was partly available in the system after Cr-spinel precipitation, giving rise to small volumes of a remnant, high temperature post-magmatic fluid (450-750 °C; e.g., Nozaka and Fryer 2011). Water [$H_2O_{(l)}$] was derived from the residual concentration of H_2 in a fluid produced after the consumption of S, present in the initial silicate melt as H_2S, to form sulphides that

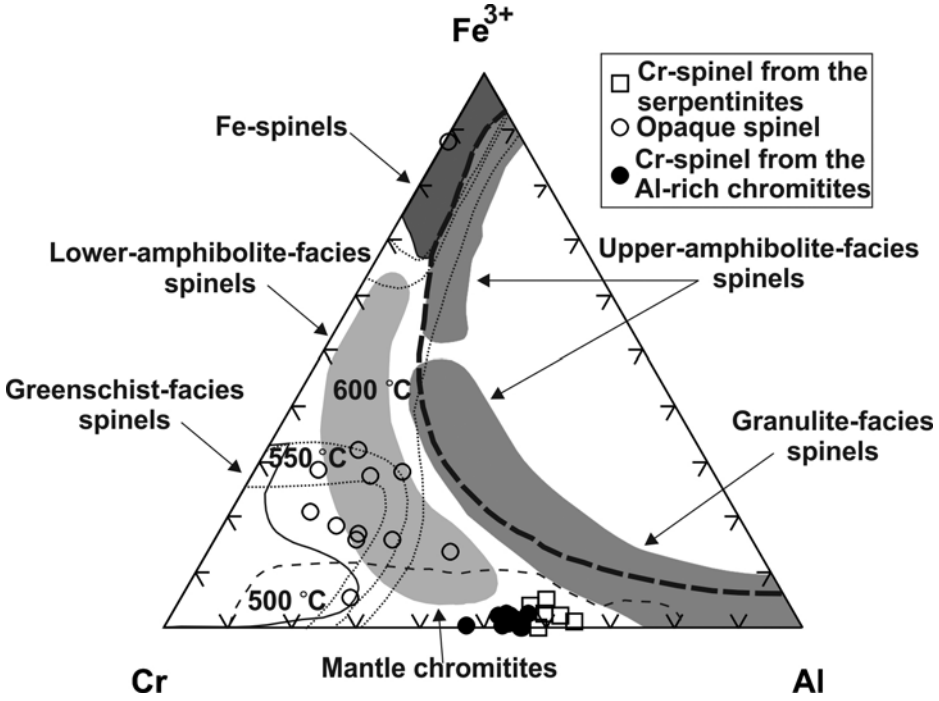

Text-fig. 7. Compositional changes in spinel phases from the Al-rich chromitite and serpentinite expressed in a Al-Fe^{3+}-Cr plot with special reference to the fields of different metamorphic facies defined for Cr-spinels by Purvis *et al*. (1972), Evans and Frost (1975) and Suita and Streider (1996). Solvus determined at 600, 550 and 500 °C by Shack and Ghiorso (1991) for Cr-spinel coexisting with olivine containing Fo_{90}

currently appear as compositionally modified BBM interstitial to Cr-spinel grains from which the Al-rich chromitite is made of (e.g., Ballhaus and Stumpfl 1986; Ferrario and Garuti 1990; Melcher *et al*. 1997). This fluid could have effectively modified the composition of Cr-spinel, although it was rapidly consumed, as is indicated by the development of narrow ferrian chromite zones in Cr-spinel and the unchanged composition of Cr-spinels in the former dunite host. Moreover, the above scenario explains satisfactorily the lack of any signs of alteration in magnesiochromite from the high-Cr chromitite. It is proposed that this high temperature post-magmatic event was overprinted by a low temperature hydrothermal episode related to serpentinization (200–300 °C; Grieco and Merlini 2011). Any possible interaction of both types of hydrothermal solutions cannot be excluded as is confirmed by the existence of altered Cr-spinels with compositions suggestive of advanced greenschist facies metamorphism (300–400 °C; e.g., Merlini *et al*. 2009; Text-fig. 7).

CONCLUDING REMARKS

The current investigation has led to the following major conclusions:

The area of Korydallos in the Pindos ophiolite complex is represented by a typical blocks-in-matrix ophiolitic mélange formation, generated by tectonic mixing processes, whereby various exotic fragments, including a chromitite-bearing, fully serpentinized peridotite block, were mixed together along the subduction interface.

Petrographic observations, Cr-spinel compositions and bulk-rock analytical data indicate that the serpentinite block represents a former spinel-bearing dunite that was formed in the mantle below a fast-spreading back-arc basin.

The high-Al chromitite pod hosted in the serpentinite fragment is composed of Cr-spinel grains randomly altered to ferrian chromite (and magnetite) and clinochlore. Textural relations, such as residual olivine replacement by clinochlore and serpentine substitution for clinochlore, suggest that the chromitite pod experienced retrograde metamorphism.

Metamorphic alteration occurred immediately after high-Al chromitite genesis due to the formation of a residual, hydrous, high temperature fluid as shown by the presence of clinochlore and tremolite in the silicate groundmass of the chromitite. Later, both types of chromitites and the surrounding peridotite were affected by ocean floor serpentinization before they finally become incorporated into the Avdella mélange.

Acknowledgements

This paper is based in part on the PhD thesis of A. Kapsiotis at the University of Patras, Greece. The author expresses his deep appreciation to those colleagues from the Department of Geology at the University of Patras who did not tire in sharing ideas. In a similar vein, the author would like to recognize the highly effective contributions of his colleagues from the School of Earth Science and Geological Engineering at Sun Yat-sen University. The author is thankful to Prof. K. Hatzipanagiotou for his encouragement and V. Kotsopoulos of the Laboratory of Electron Microscopy and Microanalysis, University of Patras, for his assistance with the microanalyses and SEM micrographs. The author is indebted to Prof. Ray Macdonald for his comments on an earlier version of the manuscript. Research was financially supported by Pythagoras I project, which is co-funded by the European Social Fund and national resources (EPEAK) and the State Scholarship Foundation of Greece (IKY).

REFERENCES

Ahmed, A.H., Arai, S. and Attia, A.K. 2001. Petrological characteristics of podiform chromitites and associated peridotites of the Pan African Proterozoic ophiolite complexes of Egypt. *Mineralium Deposita*, **36**, 72–84.

Ahmed, A.H., Harbi, H.M. and Habtoor, A.M. 2012. Compositional variations and tectonic settings of podiform chromitites and associated ultramafic rocks of the Neoproterozoic ophiolite at Wadi Al Hwanet, northwestern Saudi Arabia. *Journal of Asian Earth Sciences*, **56**, 118–134.

Arai, S. and Akizawa, N. 2014. Precipitation and dissolution of chromite by hydrothermal solutions in the Oman ophiolite: New behavior of Cr and chromite. *American Mineralogist*, **99**, 28–34.

Arai, S., Shimizu, Y., Ismail, S.A. and Ahmed, A.H. 2006. Low-T formation of high-Cr spinel with apparently primary chemical characteristics within podiform chromitite from Rayat, northeastern Iraq. *Mineralogical Magazine*, **70**, 499–508.

Azer, M.K. 2014. Petrological studies of Neoproterozoic serpentinized ultramafics of the Nubian Shield: spinel compositions as evidence of the tectonic evolution of Egyptian ophiolites. *Acta Geologica Polonica*, **64**, 113–127.

Bailey, S.W. 1980. Summary of recommendations of AIPEA nomenclature committee on clay minerals. *American Mineralogist*, **65**, 1–7.

Ballhaus, C.G. and Stumpfl, E.F. 1986. Sulfide and platinum mineralization in the Merensky Reef: evidence from hydrous silicates and fluids inclusions. *Contributions to Mineralogy and Petrol*ogy, **94**, 193–204.

Barnes, S.J. 2000. Chromite in komatiites, II. Modification during greenschist to mid-amphibolite facies metamorphism. *Journal of Petrology*, **41**, 387–409.

Beccaluva, L., Coltorti, M., Saccani, E. and Siena, F. 2005. Magma generation and crustal accretion as evidenced by supra-subduction ophiolite of the Albanide-Hellenide Subpelagonian Zone. *The Island Arc*, **14**, 551–563.

Beccaluva, L., Ohnenstetter, D., Ohnenstetter, M. and Paupy, A. 1984. Two magmatic series with island arc affinities within the Vourinos Ophiolites. *Contributions to Mineralogy and Petrology*, **85**, 253–271.

Brunn, J.H. 1956. Contribution à l'étude géologique du Pinde septentrional et d'une partie de la Macédoine occidentale. *Annales Géologiques Des Pays Helléniques*, **7**, pp. 358.

Burkhard, D.J.M. 1993. Accessory chromium spinels: Their coexistence and alteration in serpentinites. *Geochimica et Cosmochimica Acta*, **57**, 1297–1306.

Candia, M.A.F. and Gaspar, J.C. 1997. Chromian spinels in metamorphosed ultramafic rocks from Mangabal I and II complexes, Goiás, Brazil. *Mineralogy and Petrology*, **60**, 27–40.

Ceuleneer, G., Nicolas, A. and Boudier, F. 1988. Mantle flow patterns an oceanic spreading center: the Oman peridotites record. *Tectonophysics*, **151**, 1–26.

Colás, V., Gervilla, F., Fanlo, I., Kerestedjian, T., Sergeeva, I., González-Jiménez, J.M. and Arranz, E. 2012. Factors Controlling Chromite Alteration: Example from Costurino, SE Bulgaria. In: Revista de la sociedad española de mineralogia. *Revista de la sociedad española de mineralogia*, *Macla*, **16**, 238–239.

Danelian, T. and Robertson, A.H.F. 2001. Neotethyan evolution of eastern Greece (Pagondas Me´lange, Evia Island) inferred from Radiolarian biostratigraphy and the geochemistry of associated extrusive rocks. *Geological Magazine*, **138**, 345–363.

Derbyshire, E.J., O'Driscoll, B., Lenaz, D., Gertisser, R. and Kronz, A. 2013. Compositionally heterogeneous podiform chromitite in the Shetland Ophiolite Complex (Scotland): Implications for chromitite petrogenesis and late-stage alteration in the upper mantle portion of a supra-subduction zone ophiolite. *Lithos*, **162-163**, 279–300.

Dick, H.J.B. and Bullen, T. 1984. Chromian spinel as a petrogenetic indicator in abyssal and alpine-type peridotites and spatially associated lavas. *Contributions to Mineralogy and Petrology*, **86**, 54–76.

Dijkstra, A.H., Barth, M.G., Drury, M.R., Mason, P.R.D. and Vissers, R.L.M. 2003. Diffuse porous melt flow and melt-rock reaction in the mantle lithosphere at a slow-spreading ridge: A structural petrology and LA-ICP-MS study of the Othris Peridotite Massif (Greece). *Geochemistry Geophysics Geosystems*, **4**, doi: 1029/2001GC000278.

Dilek, Y., Furnes, H. and Shallo, M. 2007. Suprasubduction zone ophiolite formation along the periphery of Mesozoic Gondwana. *Gondwana Research*, **11**, 453–475.

Dubois-Côté, V., Hébert, R., Dupuis, C., Wang, C.S., Li, Y.L. and Dostal, J. 2005. Petrological and geochemical evidence for the origin of the Yarlung Zangbo ophiolites, southern Tibet. *Chemical Geology*, **214**, 265–286.

Economou-Eliopoulos, M. 2003. Apatite and Mn, Zn, Co-enriched chromite in Ni Laterites of northern Greece and their genetic significance. *Journal of Geochemical Exploration*, **80**, 41–54.

Ernst, W.G. 1993. Metamorphism of Franciscan tectonostratigraphic assemblage, Pacheco Pass area, east-central Diablo Range, California Coast Ranges. *Bulletin of the Geological Society of America*, **105**, 618–636.

Evans, B.W. and Frost, B.R. 1975. Chrome-spinel in progressive metamorphism. A preliminary analysis. *Geochimica et Cosmochimica Acta*, **39**, 959–972.

Ferrario, A. and Garuti, G. 1990. Platinum-group mineral inclusions in chromitites of the Finero mafic-ultramafic complex (Ivrea-Zone, Italy). *Mineralogy and Petrol*ogy, **41**, 125–143.

Gahlan, H.A. and Arai, S. 2007. Genesis of peculiarly zoned Co, Zn, and Mn-rich chromian spinel in serpentinite of Bou-Azzer ophiolite, Anti-Atlas, Morocco. *Journal of Mineralogical and Petrological Sciences*, **2**, 69–85.

Gervilla, F., Padrón-Navarta, J.A., Kerestedjian, T., Sergeeva, I., González-Jiménez, J.M. and Fanlo, I. 2012. Formation of ferrian chromite in podiform chromitites from the Golyamo Kamenyane serpentinite, Eastern Rhodopes, SE Bulgaria: a two stage process. *Contributions to Mineralogy and Petrology*, **164**, 643–657.

Ghikas, C., Dilek, Y. and Rassios, A.E. 2010. Structure and tectonics of subophiolitic mélanges in the western Hellenides (Greece): implications for ophiolite emplacement tectonics. *International Geology Reviews*, **52**, 423–453.

González-Jiménez, J.M., Kerestedjian, T., Proenza, J.A. and Gervilla, F. 2009. Metamorphism on chromite ores from the Dobromirtsi ultramafic massif, Rhodope mountains (SE Bulgaria). *Geologica Acta*, **7**, 413–429.

Grieco, G. and Merlini, A. 2011. Chromite alteration processes within Vourinos ophiolite. *International Journal of Earth Sciences*, **101**, 1523–1533.

Hellebrand, E., Snow, J.E., Dick, H.J.B. and Hofmann, A.W. 2001. Coupled major and trace elements as indicator of the extent of melting in mid-ocean-ridge peridotites. *Nature*, **410**, 677–681.

Hill, R.J, Craig, J.R. and Gibbs, G.V. 1979. Systematics of the spinel structure type. *Physics and Chemistry of Minerals*, **4**, 317–339.

Hoffman, E.L. 1992. Instrumental Neutron Activation in Geoanalysis. *Journal of Geochemical Exploration*, **44**, 297–319.

Ishii, T., Robinson, P.T., Maekawa, H. and Fiske, R. 1992. Petrological studies of peridotites from diapiric serpentinite seamounts in the Izu-Mariana fore-arc, Leg 125. *Pro-*

ceedings of the Ocean Drilling Project, Scientific Results, **125**, 445–485.

Jacobshagen, V. 1986. Geologie von Griechenland. Berlin, Stuttgart, Gebrüder Borntraeger, 363.

Jan, M.Q. and Windley, B.F. 1990. Chromian spinel-silicate chemistry in ultramafic rocks of the Jijal complex, Nothwestern Pakistan. *Journal of Petrology*, **31**, 667–715.

Jones, G. and Robertson, A.H.F. 1991. Tectono-stratigraphy and evolution of the Mesozoic Pindos ophiolite and related units, northwestern Greece. *Journal of the Geological Society of London*, **148**, 267–288.

Jones, G., Robertson, A.H.F. and Cann, J.R. 1991. Genesis and Emplacement of the suprasubduction zone Pindos Ophiolite, northwestern Greece. In: Ophiolite Genesis and Evolution of the Oceanic Lithosphere, Peters, T., Nicolas, A., Coleman, S. (eds.). *Sultanate of Oman: Ministry of Petroleum and Minerals*, 771–799.

Juteau T., Berger E. and Cannat M. 1990. Serpentinized, residual mantle peridotites from the M.A.R. median valley, ODP hole 670A (21º 10'N, 45º 02'W): primary mineralogy and geothermometry. *Proceedings of the Ocean Drilling Project, Scientific Results*, **106 (109)**, 27–45.

Kamenetsky, V.S., Crawford, A.J. and Meffre, S. 2001. Factors controlling chemistry of magmatic spinel: An empirical study of associated olivine, Cr-spinel and melt inclusions from primitive rocks. *Journal of Petrology*, **42**, 655–671.

Kapsiotis, A. 2013. Genesis of chromitites from Korydallos, Pindos Ophiolite Complex, Greece, based on spinel chemistry and PGE-mineralogy. *Journal of Geosciences*, **58**, 49–69.

Kapsiotis, A. 2014. Composition and alteration of Cr-spinels from Milia and Pefki serpentinized mantle peridotites, Pindos Ophiolite Complex, Greece. *Geologica Carpathica*, **65**, 83–95.

Kapsiotis, A., Grammatikopoulos, T.A., Tsikouras, B. and Hatzipanagiotou, K. 2010. Platinum-group mineral characterization in concentrates from high-grade PGE Al-rich chromitites of Korydallos Area in the Pindos Ophiolite Complex (NW Greece). *Resource Geology*, **60**,178–191.

Kimball, K.L. 1990. Effects of hydrothermal alteration on the composition of chromian spinels. *Contributions to Mineralogy and Petrology*, **105**, 337–346.

Kostopoulos, D.K. 1989. Geochemistry, petrogenesis and tectonic setting of the Pindos Ophiolite, NW Greece. Unpublished Ph.D. Thesis, University of Newcastle, Newcastle, UK, 1–468.

Leake, B.E. and 20 others 1997. Nomenclature of amphiboles: report of the subcommittee on amphiboles of the international mineralogical association, commission of new minerals and mineral names. *The Canadian Mineralogist*, **35**, 219–246.

Liati, A., Gebauer. D. and Fanning., C.M. 2004. The age of ophiolitic rocks of the Hellenides (Vourinos, Pindos, Crete): first U-Pb ion microprobe (SHRIMP) zircon ages. *Chemical Geology*, **207**, 171–188.

Melcher, F., Grum, W., Simon, G., Thalhammer, T.V. and Stumpfl, E.F. 1997. Petrogenesis of the ophiolitic giant chromite deposits of Kempirsai, Kazakhstan: a study of solid and fluid inclusions in chromite. *Journal of Petrology*, **38**, 1419–1458.

Mellini, M., Rumori, C. and Viti, C. 2005. Hydrothermally reset magmatic spinels in retrogade serpentinites: Formation of "ferritchromit" rims and chlorite aureoles. *Contributions to Mineralogy and Petrology*, **149**, 266–275.

Merlini, A., Grieco, G. and Diella, V. 2009. Ferritchromite and chromian-chlorite formation in mélange-hosted Kalkan chromitite (Southern Urals, Russia). *American Mineralogist*, **94**, 1459–1467.

Mukherjee, R., Mondal, S.K., Rosing, M.T. and Frei, R. 2010. Compositional variations in the Mesoarchean chromitites of the Nuggihalli schist belt, Western Dharwar Craton (India): potential parental melts and implications for tectonic setting. *Contributions to Mineralogy and Petrology*, **160**, 865–885.

Myhill, R. 2011. Constraints on the evolution of the Mesohellenic Ophiolite from subophiolitic metamorphic rocks. In: Mélanges: Processes of Formation and Societal Significance, Wakabayashi, J., Dilek Y. (Eds). *Geological Society of America Special Papers*, **480**, 75–94.

Nicolas, A. 1986. Structure and petrology of peridotites: Clues to their geodynamic environment. *Review Geophysics*, **27**, 999–1022.

Nicolas, A. 1989. In: Structures of ophiolites and dynamics of oceanic lithosphere. Kluwer Academic, Dordrecht, The Netherlands, 367.

Nozaka, T. and Fryer, P. 2011. Alteration of the oceanic lower crust at a slow-spreading axis: insight from vein-related zoned halos in olivine gabbro from Atlantis Massif, Mid-Atlantic Ridge. *Journal of Petrology*, **52**, 643–664.

Ohara, Y. 2006. Mantle process beneath Philippine Sea back-arc spreading ridges: A synthesis of peridotite petrology and tectonics. *The Island Arc*, **15**, 119–129.

Ohara, Y. and Ishii, T. 1998. Peridotites from the southern Mariana forearc: heterogeneous fluid supply in the mantle wedge. *The Island Arc*, **7**, 541–558.

Ohara, Y., Stern, R.J., Ishii, T., Yurimoto, H., Yamazaki, T. 2002. Peridotites from the Mariana trough: First look at the mantle beneath an active back-arc basin. *Contributions to Mineralogy and Petrology*, **143**, 1–18.

Pawley, A. 2002. Chlorite stability in mantle peridotite: the reaction clinochlore + enstatite = forsterite + pyrope + H2O. *Contributions to Mineralogy and Petrology*, **144**, 449–456.

Pelletier, L., Vils, F., Kalt, A. and Gmeling, K. 2008. Li, B and Be Contents of Harzburgites from the Dramala Complex (Pindos Ophiolite, Greece): Evidence for a MOR-type Mantle in a Supra-subduction Zone Environment. *Journal of Petrology*, **49**, 2043–2080.

Prichard, H., Economou-Eliopoulos, M. and Fisher, P.C. 2008. Contrasting platinum-group mineral assemblages from two different podiform chromitite localities in the Pindos ophiolite complex, Greece. *The Canadian Mineralogist*, **46**, 329–341.

Proenza, J.A., Gervilla, F., Melgarejo, J.C. and Bodinier, J.L. 1999. Al- and Cr-rich chromitites from the Mayarí-Baracoa ophiolitic belt (eastern Cuba): Consequence of interaction between volatile-rich melts and peridotites in suprasubduction mantle. *Economic Geology*, **94**, 547–566.

Purvis, A.C., Nesbitt, R.W. and Hallberg, J.A. 1972. The geology of part of the Carr Boyd rocks complex and its associated nickel mineralization, Western Australia. *Economic Geology*, **67**, 1093–1113.

Rassios, A. 1991. Internal structure and pseudostratigraphy of the Dramala peridotite massif, Pindos mountains, Greece. *Bulletin of the Geological Society of Greece*, **25**, 293–305.

Robertson, A.H.F., Clift, P.D., Degnan, P.J. and Jones, G. 1991. Palaeogeographic and palaeotectonic evolution of the Eastern Mediterranean Neotethys. *Palaeogeography, Palaeoclimatology, Palaeoecology*, **87**, 289–343.

Robertson, A.H.F. 2002. Overview of the genesis and emplacement of Mesozoic ophiolites in the Eastern Mediterranean Tethyan region. *Lithos*, **65**, 1–67.

Ross, J.V. and Zimmerman, J. 1996. Comparison of evolution and tectonic significance of the Pindos and Vourinos ophiolite suites, northern Greece. *Tectonophysics*, **256**, 1–15.

Saccani, E., Beccaluva, L., Coltorti, M. and Siena, F. 2004. Petrogenesis and tectono-magmatic significance of the Albanide-Hellenide ophiolites. *Ofioliti*, **29**, 77–95.

Saccani, E., Beccaluva, L., Photiades, A. and Zeda, O. 2011. Petrogenesis and tectono-magmatic significance of basalts and mantle peridotites from the Albanian-Greek ophiolites and sub-ophiolitic mélanges. New constraints for the Triassic-Jurassic evolution of the Neo-Tethys in the Dinaride sector. *Lithos*, **124**, 227–242.

Saumur, B.M. and Hattori, K. 2013. Zoned Cr-spinel and ferritchromite alteration in forearc mantle serpentinites of the Rio San Juan Complex, Dominican Republic. *Mineralogical Magazine*, **77**, 117–136.

Shack, R.O. and Ghiorso, M.S. 1991. Chromian spinels as petrogenetic indicators: thermodynamic and petrological applications. *American Mineralogist*, **76**, 827–847.

Singh, A.K. and Singh, R.B. 2013. Genetic implications of Zn- and Mn-rich Cr-spinels in serpentinites of the Tidding Suture Zone, eastern Himalaya, NE India. *Geological Journal*, **48**, 22–38.

Snow, J. and Dick, H.B.J. 1995. Pervasive magnesium loss by marine weathering of peridotites. *Geochimica et Cosmochimica Acta*, **59**, 4219–4235.

Sobolev, N.V. and Logvinova, A.M. 2005. Significance of accessory chrome spinel in identifying serpentinite paragenesis. *International Geology Review*, **47**, 58–64.

Spangenberg, K. 1943. Die chromitlagerstätte von Tampadel in Zobten. *Zeitschrift Praktische Geologie*, **51**, 13–35.

Spary, J.G., Bebien, J., Rex, D.C. and Roddick, J.C. 1984. Age constraints on the igneous and metamorphic evolution of the Hellenic-Dinaric ophiolites. In: The Geological Evolution of the Eastern Mediterranean, Dixon, J.E., Robertson, A.H.F. (eds.). *Geological Society of London Special Publications*, **17**, 619–627.

Stanton, R.L. 1972. Ore petrology. In: International Series in the Earth and Planetary Science. *McGraw-Hill, New-York*, 1–713.

Stern, C.R. and Elthon, D.L. 1979. Vertical variations in the effects of hydrothermal metamorphism in Chilean ophiolitew: Their implications for ocean floor metamorphism. *Tectonophysics*, **55**, 179–213.

Suhr, G. 1993. Evaluation of upper mantle microstructures in the Table Mountain Massif (Bay of Islands ophiolite). *Journal of Structural Geology*, **15**, 1273–1292.

Suita, M.T.F. and Streider, A.J. 1996. Cr-spinel from Brazilian mafic-ultramafic complexes: Metamorphic modifications. *International Geological Review*, **38**, 245–267.

Sun, S.S. and Nesbitt, R.W. 1977. Chemical Heterogeneity of Archaean Mantle, Composition of Earth and Mantle Evolution. *Earth and Planetary Science Letters*, **35(3)**, 429-448.

Tarkian, M., Economou-Eliopoulos, M. and Sambanis, G. 1996. Platinum-group minerals in chromitites from the Pindos ophiolite complex, Greece. *Neues Jahrbuch für Mineralogie*, **4**, 145–160.

Teixeira, R.J.S., Neiva, A.M.R. and Gomes, M.E.P. 2012. Chromian spinels and magnetite of serpentinites, steatitic rocks, tremolite asbestos and chloritites from Bragança massif, northeastern Portugal. *Periodico di Mineralogia*, **81**, 237–256.

Thuizat, R., Whitechurch, H., Montigny, R. and Juteau, T. 1981. K-Ar dating of some infra-ophiolitic metamorphic soles from the Eastern Mediterranean: new evidence for ocean thrusting before obduction. *Earth and Planetary Science Letters*, **52**, 301–310.

Ulmer, G.C. 1974. Alteration of chromite during serpentinization in the Pennsylvania-Maryland district. *American Mineralogist*, **59**, 1236–1241.

Wood, B.J., Kirpatrick, R.J and Montez, B. 1986. Order-disorder phenomena in $MgAl_2O_4$ spinel. *American Mineralogist*, **71**, 999–1006.

Wylie, A.G., Candela, P.A. and Burkle, T.M. 1987. Compositional zoning in unusual Zn-rich chromite from the Sykeville district of Maryland and its bearing on the origin of the ferritchromit. *American Mineralogist*, **72**, 413–422.

Xiong, F., Yang, J., Robinson, P.T., Xu, X., Liu, Z., Li, Y., Li, J. and Chen, S. 2014. Origin of podiform chromitite, a new model based on the Luobusa ophiolite, Tibet. *Gondwana Research*, 10.1016/j.gr.2014.04.008.

Zhou, M-F., Robinson, P.T., Malpas, J., Edwards, S.J. and Qi, L. 2005. REE and PGE geochemical constraints on the formation of dunites in the Luobusa ophiolite, Southern Tibet. *Journal of Petrology*, **46**, 615–639.

Manuscript submitted: 30th May 2014
Revised version accepted: 10th October 2014